



Dalton  
Transactions

**Blocking Like It's Hot: A Synthetic Chemists' Path to High-Temperature Lanthanide Single Molecule Magnets**

Journal:	<i>Dalton Transactions</i>
Manuscript ID	DT-FRO-05-2020-001904.R2
Article Type:	Frontier
Date Submitted by the Author:	10-Sep-2020
Complete List of Authors:	Goodwin, Conrad; Los Alamos National Laboratory, C-IIAC

SCHOLARONE™  
Manuscripts

## Blocking Like It's Hot: A Synthetic Chemists' Path to High-Temperature Lanthanide Single Molecule Magnets

Conrad A. P. Goodwin\*†

### Abstract

Progress in the synthesis, design, and characterisation of single-molecule magnets (SMMs) has expanded dramatically from curiosity driven beginnings to molecules that retain magnetization above the boiling point of liquid nitrogen. This is in no small part due to the increasingly collaborative nature of this research where synthetic targets are guided by theoretical design criteria. This article aims to summarize these efforts and progress from the perspective of a synthetic chemist with a focus on how chemistry can modulate physical properties. A simple overview is presented of lanthanide electronic structure in order to contextualize the synthetic advances that have led to drastic improvements in the performance of lanthanide-based SMMs from the early 2000s to the late 2010s.

### Introduction

An SMM can be viewed simply as a nanoscopic bar magnet: a molecule whose magnetic moment can be manipulated, to be programmed or read out as desired, with the underlying physics determined by molecular structure. Between 1993 and 2020 there have been breath-taking advancements in our understanding of how to control magnetic properties through synthetic chemistry. This has been driven by sound theoretical principles and a growing understanding of the underlying physics of molecular magnetism.<sup>1</sup> The first molecule found to possess properties reminiscent of a conventional hard ferromagnet was the multimetallic d-block complex  $[\text{Mn}_{12}\text{O}_{12}(\text{OAc})_{16}(\text{H}_2\text{O})_4]$  (**1**, commonly referred to as “ $\text{Mn}_{12}\text{OAc}$ ” or simply “ $\text{Mn}_{12}$ ”; Figure 1,  $\text{OAc} = \{\text{CH}_3\text{COO}\}$ ).<sup>2</sup> First synthesized by Lis in 1980,<sup>3</sup> it was thirteen years later that Sessoli, Gatteschi, and Caneschi showed that **1** did not entirely behave as a simple paramagnet at all temperatures, but rather was able to retain its magnetic moment without an applied field at extremely low temperatures (4 K). The concluding sentences of that paper have defined the field: “If a means is found of properly addressing individual clusters it might then be possible to store information at the molecular level – albeit at temperatures no greater than about 4 K in this case”.<sup>2</sup> The read/write-ability of individual SMMs is paramount to their technological utility, though is beyond the scope of this article and readers are directed to several other works.<sup>4-8</sup> Instead, here the focus is on the second part of this statement – the need to maintain the magnetic moment at temperatures greater than 4 K. While this is an enormous task, it has been tackled in practical ways through molecular design guided by experimental evidence and theoretical predictions, and lanthanide (Ln) ions have emerged as promising candidates for realising this goal.<sup>9-12</sup> Various resources including textbooks and tutorial reviews can provide the reader with a more in-depth background on the fundamentals behind magnetic materials and molecules,<sup>13-21</sup> indeed the breadth of work in this area can be overwhelming. Beyond magnetic storage prospects, these materials can also be used to build nanoscale devices, and to solve fundamental physics questions in a variety of settings and this area has also been nicely summarised by Coronado, Sessoli and Gatteschi.<sup>22-25</sup>

---

† Chemistry Division, Los Alamos National Laboratory, NM, USA 87545

This article aims to showcase some modern advances in the development of Ln SMMs from a synthetic chemists' perspective to provide a narrative on the natural progression of the research field that has resulted in magnetic remanence at unprecedentedly high temperatures. Molecular magnetism is a broad and diverse field, and the topics laid out below are not the only important areas that have contributed to the current state of research. Contributions from elsewhere in the periodic table (e.g. transition metals and p-block radicals, or mixed-metal systems) should not be ignored as they have increased our fundamental understanding of magnetic phenomena,<sup>26,27</sup> though it is not possible to encapsulate the field in its entirety across the whole periodic table in a single article. To help contextualise how the intersection of synthesis and theory has led to significant progress in recent years, an introduction to some of the underlying electronic structure features is also provided.

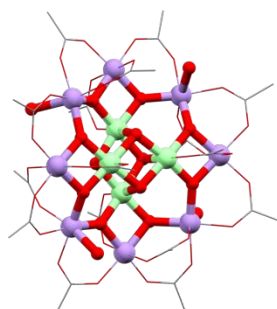


**Figure 1.** Mn<sub>12</sub>OAc (**1**), H<sub>2</sub>O molecules and H atoms removed for clarity. Mn<sup>4+</sup> = light green, Mn<sup>3+</sup> = purple, C = grey, O = red. OAc = {CH<sub>3</sub>COO}.

## Discussion

### *Anisotropy, electronic structure, and magnetic blocking*

Early design principles for d-block SMMs relied on a large total spin,  $S$ , and favourable axial magnetic anisotropy (negative, easy-axis-type,  $g_z > g_{xy}$ ),  $D$ , which together can be related to the thermal barrier to the reversal of magnetization,  $U_{\text{eff}}$ : for integer  $S$ ,  $U_{\text{eff}} = S^2|D|$ ; and non-integer  $S$ ,  $U_{\text{eff}} = (S^2 - 1/4)|D|$  spin systems. These relationships arise from the simplified Hamiltonian  $\hat{H} = [D\hat{S}_z^2 - S(S+1)/3 + E(\hat{S}_x^2 - \hat{S}_y^2)]$  where  $\hat{S}_x/y/z$  are spin operators describing the spin projection along each axis; while  $D$  and  $E$  are the axial and rhombic zero-field splitting parameters, respectively. This would suggest that increasing  $S$  would improve  $U_{\text{eff}}$ , and thus large multi-metallic systems are desirable, however after the preparation of many large-spin-ground-state molecules,<sup>28-34</sup> it was found that when  $D$  arises due to spin orbit coupling (SOC), it is inversely proportional to  $S^2$ .<sup>35</sup> Therefore molecules maximising  $D$  should be targeted instead, for which Ln ions are well suited.<sup>12,14,16</sup>

A free ion has no anisotropy as it is spherically symmetric, however, the presence of ligands leads to splitting of degenerate orbitals (crystal field (CF) splitting). The resultant electronic structures are very different for 3d-block and Ln ions (Figure 2 for the Ln case). In 3d-block complexes such as **1**, the crystal field (CF) splitting is large ( $\sim 10 - 35,000 \text{ cm}^{-1}$ ), and breaks the degeneracy between some or all of the 3d orbitals depending on local symmetry. Where the ground state is orbitally-degenerate and has non-zero orbital angular momentum, SOC splits the CF terms into states classified by total angular momentum,  $J$ , which each consist of  $2J+1 m_J$  states. When the ground term has no orbital angular momentum, there can still be a small zero-field splitting (ZFS) between the  $m_s$  states due to second-order SOC with excited states. For Ln ions the CF

interaction is much smaller ( $\sim 1 - 2,000 \text{ cm}^{-1}$ ), so that SOC dominates and splits the ground state into well-defined  $J$  multiplets, which are then split by the CF into  $2J+1$   $m_J$  components. Due to these electronic factors, single Ln ions have the potential for values of  $D$  that are at least an order of magnitude larger than most 3d-block ions while also having intrinsically large  $J$  for the mid-late 4f series. Even the first Ln SMM  $[\text{N}(\text{nBu})_4][\text{Tb}(\text{Pc})_2]$  reported by Ishikawa in 2003 (**2-Tb**;  $\text{nBu} = \text{}^n\text{C}_4\text{H}_9$ , Pc = phthalocyanine),<sup>36,37</sup> demonstrated a larger  $U_{\text{eff}}$  value than most TM clusters ( $230 \text{ cm}^{-1}$  in **2-Tb** *c.f.*  $42 \text{ cm}^{-1}$  in **1**), and the area of Ln-based SMMs has blossomed since.<sup>38,39</sup> Some remarkable exceptions to this generalization are based on highly axial  $\text{Fe}^+$  and  $\text{Co}^{2+}$  complexes with relatively large  $U_{\text{eff}}$  values by virtue of exceptionally weak ligand fields which don't fully quench the orbital angular momentum;<sup>40-42</sup> though Ln-based SMMs are the central focus herein.

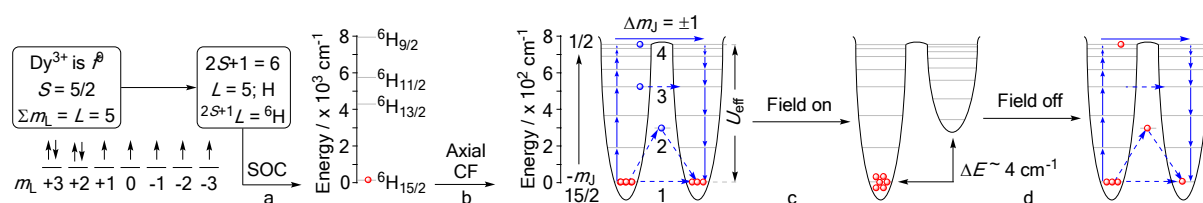


**Figure 2.** Electronic interactions for a  $\text{Dy}^{3+}$  ion in an axial crystal field. Red circles show electronic populations in a sample, blue circles are a visual aid for the relaxation processes which are denoted by blue arrows. a) Spin orbit coupling (SOC) splits the Russell-Saunders  ${}^6\text{H}$  ground term into  $J$  states ( $J = |L-S| \dots L+S$ ;  $\Delta J = 1$ ) – for  $\text{Dy}^{3+}$  this is  ${}^6\text{H}_{15/2} \dots {}^6\text{H}_{5/2}$ ; b) In a crystal field, each  $J$  state is split into  $2J+1$   $m_J$  states; c) Application of an external magnetic field changes the energies of the  $m_J$  states (not to scale) and biases the electronic population; d) Removal of the external field allows the electronic population to relax back to equilibrium *via* several mechanisms: 1) quantum tunnelling of magnetisation (QTM), a through-barrier process that can occur at the ground state; 2) *via* virtual states in a 2-phonon (Raman) process; 3) thermally assisted quantum tunnelling of magnetisation (TA-QTM), which is QTM *via* excited  $m_J$  states; 4) a stepwise thermally activated (Orbach) process over the  $U_{\text{eff}}$  barrier (in real systems  $U_{\text{eff}}$  does not necessarily coincide with the most energetic  $m_J$  states).

In practice while the  $U_{\text{eff}}$  is an important measure of the ability of an SMM to retain magnetization, traversing over the barrier does not represent the only pathway to relaxation (Figure 2), thus strategies designed to hinder all of them have been developed and will be discussed below.<sup>43-45</sup> It is convenient to describe the splitting of the ground  ${}^6\text{H}_{15/2}$  term (for  $\text{Dy}^{3+}$ ) into well-defined  $m_J$  states as in Figure 2, however in the absence of a perfectly axial CF there is always a degree of mixing between the definite  $m_J$  projections. In cases where this mixing is considerable it is inappropriate to label states as  $m_J$ , and instead the expectation value of the operator  $\langle \hat{J}_z \rangle$  could be a useful label. This is simply the linear combination of wavefunction contributions to each of the Kramers doublets and is convenient as it is proportional to the magnetic moment, which can be measured directly. In this article  $m_J$  labels (Figure 3) are used when a state is almost entirely described by a single contribution (>96%). Numerous other works provide further approachable introductory material and historical perspectives to the topic of d-block, Ln, or even actinide SMMs.<sup>16,38,46-55</sup>

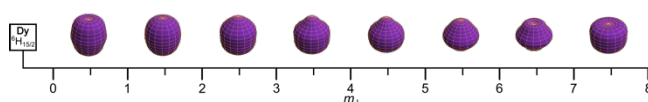


**Figure 3.** Angular dependence of the 4f electron density for the  $m_J$  states of the ground  ${}^6H_{15/2}$  multiplet of  $Dy^{3+}$ , adapted from reference 56 and 57.

The coupling of spins and phonons further complicates the simple model in Figure 2, and a recent article explores the complex theoretical background behind this.<sup>58</sup> In a perfectly stationary molecule in a crystalline lattice, akin to a picture on a page, it is not only the charges on bound ligands, but also the presence of lattice solvent molecules and counterions that effect the electric field about the metal and hence the energies of the  $m_J$  states. The vibrational and translational modes of all of these components are the source of phonons (quanta of energy) for  $\pm m_J$  transitions.<sup>59</sup> If there are no phonons of appropriate energy to facilitate a transition between  $m_J$  states, it should be blocked; for example if  $m_J = \pm 13/2$  sits  $300\text{ cm}^{-1}$  above  $m_J = \pm 15/2$  and there are no phonon modes at this energy available within the lattice, then this transition could be blocked. In a real system, as these molecular motions occur, they also perturb the electric field and subtly change the energies of individual  $\pm m_J$  levels from that of our static model. Even at mK temperatures nothing is completely stationary, and thus the first excitation gap described above would deviate slightly from  $300\text{ cm}^{-1}$  as a function of the amplitude of atomic displacements (and hence electric field modulation) during things such as ligand vibrational modes (e.g. a Dy–N stretch for a Dy amide complex). Thus, we need to consider a wider range of phonon energies that may be able to couple to the excitation gaps as the gaps themselves are not energetically fixed. The presence of a large number of low energy ligand vibrational modes, such as when flexible ligands are present, essentially guarantees that there will be some optical phonons of close-enough energy that will couple with the spin and affect relaxation at undesirable temperatures. While single-atom approaches to magnetic bistability are promising and obviate some of the complexities of coordination chemistry, they are exceedingly difficult to realize at-scale.<sup>60,61</sup>

Articles by Sievers,<sup>62</sup> Long,<sup>56</sup> and Tong,<sup>17</sup> have conveniently served to illustrate how molecular geometry, and hence the CF, of a complex interacts with the  $m_J$  states of an  $Ln^{3+}$  ion; to this end, the size of  $U_{\text{eff}}$  is proportional to the strength of the CF in relation to the projections of the  $m_J$  states. For example, theoretical work by Ungur and Chibotaru has shown that in the case of a hypothetical two-coordinate  $Dy^{3+}$  molecule, ligand(s) solely along the z-axis would in principle create the largest difference between the  $m_J = \pm 15/2$  and  $m_J = \pm 1/2$  states because the ligand electric field is well-placed to destabilize  $m_J = \pm 1/2$  whilst stabilizing  $m_J = \pm 15/2$  (Figure 3).<sup>63,64</sup> Minimizing off-axis contributions ensures sequential ordering and purity of these states. It is important to note that this it is strictly the disposition (and relative donor strength) of the ligands that is important with regards to the ordering of the crystal field states, and hence for establishing any potential  $U_{\text{eff}}$ . In a perfectly linear  $[Dy(CHR_2)(NR_2)]^+$  (R = any substituent) molecule there might be no symmetry beyond a mirror plane bisecting N–Dy–C(H), but this arrangement would still result in the stabilization of  $m_J = \pm 15/2$ , and destabilization of  $m_J = \pm 1/2$ . This electronic structure results in “easy-axis” anisotropy for  $Dy^{3+}$ . The word axis here does not refer to the ligand disposition but instead to the energy potential of this electronic state interacting with an external field. The potential energy of  $Dy^{3+}$   $m_J = \pm 15/2$  interacting with an external magnetic field reaches a minimum/maximum when it is aligned parallel/antiparallel with the external field hence  $g_z > g_{xy}$ . The opposite to

this can be illustrated by a hypothetical 2-coordinate perfectly linear  $[\text{Er}(\text{L})_2]^+$  complex which would likely result in an  $m_J = \pm 1/2$  ground state which for  $\text{Er}^{3+}$  has  $g_{xy} > g_z$  and thus would have “easy-plane” anisotropy. The potential energy would reach a maximum when parallel and also antiparallel with the external field, but is at a minimum when the field is normal to the  $m_J = \pm 1/2$  plane.<sup>13,19</sup> Axial anisotropy, where the ground state configuration has  $g_z > g_{xy}$  is a prerequisite for SMM behavior, but many other factors such as ligand vibrational modes and symmetry elements dictate the relaxation mechanisms between CF states once an external field is removed. It should be noted that “low symmetry” never means “no symmetry”, as any real system will have some form of symmetry or anisotropy in the ligand field and thus there will be some splitting of the CF states; as before, a free ion in zero-field would have all CF states equal in energy.

For Kramers (odd electron count) ions such as  $\text{Dy}^{3+}$ , Kramers theorem enforces twofold degeneracy of each  $\pm m_J$  state in zero-field and thus QTM between pure Kramers doublet (KD,  $m_J = \pm 15/2$  for example) is strictly forbidden and a bistable (Ising-type) ground state is ensured. This means equilibrium is reached *via* 1) sequential excitation over the barrier in the Orbach process; 2) Raman processes *via* virtual excited states; 3) thermally assisted QTM *via* excited KDs. For non-Kramers ions (such as  $\text{Tb}^{3+}$ ) a bistable ground state is only enforced in the presence of high and rigorously strict local symmetry leading to cancellation of off-axis terms, often the states that arise can be termed *pseudo*-doublets when the CF is well-quantized along a single axis, or in high symmetry.<sup>36</sup> The presence of nearby spins (such as other magnetic molecules) produces a dipolar magnetic field which can enable QTM even in Kramers ions as the degeneracy of the ground-state doublet is lifted. This effect is usually small, *ca.*  $0.2 \text{ cm}^{-1}$  for  $\text{Dy}^{3+}$  ions  $\sim 12.5 \text{ \AA}$  apart, but degeneracy is still lifted and QTM can occur. This effect can be reduced by dipolar dilution such as by co-crystallization within a diamagnetic matrix, e.g. the  $\text{Y}^{3+}$  analogue for  $\text{Dy}^{3+}$  complexes, though in practice it is impossible to eliminate all stray dipolar fields.

A further perturbation to the electronic structure occurs through hyperfine interactions of the electron-spin, with the nuclear spin ( $I$ ) on both metal and ligand atoms. For example, Ho has one >99.9% naturally abundant isotope,  $^{165}\text{Ho}$ , with  $I = 7/2$ , and the ground state term symbol for  $\text{Ho}^{3+}$  is  $^5I_8$ , which results in each  $m_J$  state being split into a total of  $(2I+1)$  hyperfine states. For  $^{165}\text{Ho}^{3+}$  there would be 16 hyperfine states ( $|\pm m_J, \pm I \rangle$ ) arising from a supposed  $m_J = \pm 8$  pair, with 8 non-degenerate  $\pm I$  levels each; this would be repeated for each *pseudo*-doublet. A Zeeman splitting diagram can be constructed that takes this into account (Figure 4). Rather than crossing (red and blue lines), QTM from  $|-m_J, -I\rangle$  to  $|+m_J, -I\rangle$  can occur (green arrow) as the external field is swept. As this removes the degeneracy of  $\pm m_J$  states even at zero-field, Kramers ions can undergo QTM. For a single ( $I \neq 0$ ) isotope of a metal there are external field strengths where QTM is enhanced,<sup>65</sup> or it can suppress QTM at zero-field,<sup>66</sup> or provide insight towards different relaxation phenomena altogether.<sup>67</sup> Several works have shown that the nuclear spin at Dy, and on ligand heteroatoms, has a measurable impact on the zero-field relaxation in different isotopomers,<sup>68-71</sup> but that other effects such as exchange interactions can be large enough to mask these effects.<sup>72</sup> While the role of nuclear hyperfine interactions is not in question, the molecules studied in these works typically have small  $U_{\text{eff}}$  values (*ca.*  $<70 \text{ cm}^{-1}$ ), and thus even at the lowest temperatures the effect of Orbach relaxation cannot always be discounted. By studying complexes with large  $U_{\text{eff}}$  (e.g.  $>800 \text{ cm}^{-1}$ ) at very low temperature, the Orbach mechanism can be essentially ignored and thus at  $\sim 2 \text{ K}$  only QTM dictates relaxation rates. Some studies have shown that even in these large-barrier molecules, the use of isotopically pure  $^{164}\text{Dy}$  ( $I = 0$ ), and magnetically dilute ( $\sim 5\% \text{ Dy@Y}$ ) samples does not completely remove

zero-field QTM steps.<sup>73</sup> Instead, correlations have been demonstrated between “molecular rigidity”, the density of states of low energy molecular vibrations that also couple to the electronic spin, and the presence of sharp zero-field steps;<sup>73-75</sup> it has recently been suggested that vibrations can open up tunnelling gaps of their own accord,<sup>76</sup> and hence these results point towards theories of vibrationally-driven QTM.

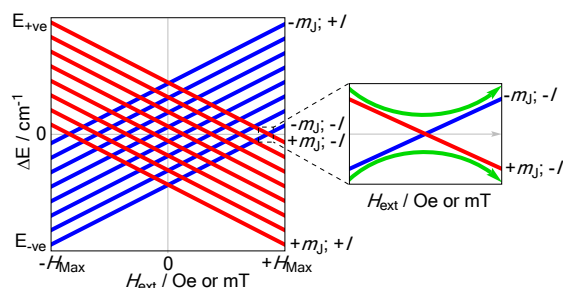


**Figure 4.** A stylised depiction of a Zeeman energy diagram for the lowest doublet of an atom ( $^{165}\text{Ho}^{3+}$ ,  $5I_8$ ) with a  $J = 8$  ground state ( $\pm m_J = 8$ ) and  $I = 7/2$  in the presence of an external magnetic field along the z-axis and an arbitrary hyperfine coupling term ( $A_{\text{hf}}$ ).<sup>65</sup> Zoomed area shows an avoided crossing between two hyperfine levels that can allow adiabatic passage from  $+m_J$  to  $-m_J$  when the external field is swept through the avoided crossing.

Phthalocyanine-based SMMs have greatly contributed to our understanding of Ln electronic structure and magnetic relaxation mechanisms.<sup>36,77</sup> However, most examples contain non-Kramers  $\text{Tb}^{3+}$  and thus are usually in-field SMMs which require an external field to suppress QTM.<sup>78-80</sup> Despite this shortcoming, the rigorous  $D_{4d}$  symmetry of Tb-phthalocyanine complexes has inspired further diverse motifs such as polyoxometallates as ligands for Ln<sup>3+</sup> ions, e.g.  $\{\text{W}_5\text{O}_{18}\}^{6-}$ .<sup>81,82</sup> Another promising avenue to constrain local geometry is to sequester Ln<sup>3+</sup> ions inside highly symmetric MOFs where the rigid framework could enforce specific symmetries at the Ln.<sup>83</sup> Ln multi-metallic cage and cluster complexes, or mixed 3d/4f systems,<sup>84-87</sup> could hold promise by analogy to 3d-block SMMs,<sup>88-95</sup> however they suffer from the same issues: greater total spin,  $S$  is inversely proportional to  $D$  and thus large  $U_{\text{eff}}$  values are hard to realise.<sup>28-33,96</sup> These observations have led to well-described design criteria for Ln-based SMMs:<sup>35,97-100</sup> i.e. Kramers ions that have highly magnetic ground states ( $\text{Dy}^{3+}$ ,  $\text{Er}^{3+}$ ) with appropriate ligand-field geometry,<sup>9-11</sup> or, non-Kramers ions combined with rigorously high-symmetry environments ( $\text{Tb}^{3+}$ ,  $\text{Ho}^{3+}$ ). Other Lns such as  $\text{Tm}^{3+}$  and  $\text{Yb}^{3+}$  have unique spectroscopic handles and can aid our understanding of Ln electronic structure through combined magnetic-photophysical studies.<sup>101,102</sup> The combination of single-crystal susceptibility measurements and luminescence can afford a detailed understanding of the ground state splitting and anisotropy axis even in  $\text{Dy}^{3+}$  which is typically only weakly luminescent,<sup>103,104</sup> and such studies have been foundational to our understanding of magnetic anisotropy in Ln ions.

#### How do you measure a magnet?

It is essential to compare SMMs consistently. The SMM community has coalesced around several figures of merit largely borrowed from the study of superparamagnetic nanoparticles. Some of these include: 1) the effective energy barrier to reversal of magnetisation ( $U_{\text{eff}}$ ), typically quoted in units of K or  $\text{cm}^{-1}$ ;‡ 2) the

‡ Values quoted in  $\text{cm}^{-1}$  rather than K can help provide clarity between energy values, and temperature.

temperature at which the zero field cooled (ZFC) susceptibility reaches a maximum ( $T_{B1}$ ); 3) the “100 s blocking temperature” ( $T_{B2}$ ), the temperature at which the relaxation time ( $\tau$ ) is 100 seconds; 4) the maximum temperature at which hysteresis is observable ( $T_H$ ). Of these four,  $U_{\text{eff}}$  and  $T_{B2}$  are the gold standards for comparison, and are the most frequently used to compare different molecules between different experimental groups.  $U_{\text{eff}}$  is determined from fits of relaxation times (Figure 5a) from AC susceptibility measurements.<sup>105</sup> Values for  $T_{B2}$  are recovered from AC susceptibility measurements and DC magnetisation decay. However, this value is not always within the experimental window of either measurements,<sup>106</sup> and results should not be extrapolated due to the confluence of multiple relaxation processes that could be fitted incorrectly,<sup>107</sup> or due to other relaxation mechanisms yet to be observed.

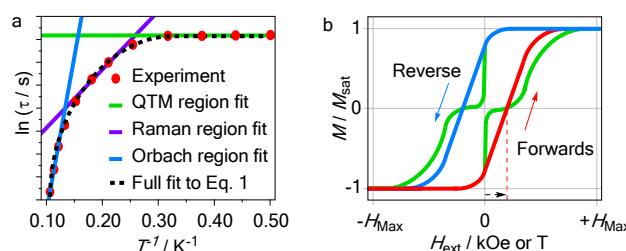


**Figure 5.** a) Stylised depiction of  $\ln(\tau)$  vs  $T^{-1}$  ( $\tau$  in s,  $T$  in K) for a hypothetical SMM, showing low temperature (green line, constant rate, QTM) fit, intermediate temperature (purple line, Raman) fit, high temperature (blue line, Orbach) fit, and a full idealized fit (dotted line) to Eq. 1; b) Stylised depiction of a magnetic hysteresis plot for a fictitious SMM. Red line represents a forward scan, blue line represents the reverse scan, green line shows a different SMM with a pronounced drop at zero-field (QTM), which is “waist-restricted” or “butterfly-shaped”.

Metrics such as  $T_{B1}$  and  $T_H$  depend on temperature, or field sweep rate, thus barring identical (or close) experimental conditions, the reader is cautioned against universally comparing these values. A fast sweep rate about the zero-field point while measuring a hysteresis loop (Figure 5b) can lead to open loops at erroneously high temperatures when compared to literature examples. There are other metrics which serve specific purposes, for example a recent criterion is the relaxation time at which the Orbach mechanism dominates over the Raman mechanism ( $\tau_{\text{switch}}$ ). This is useful for comparing series of closely related molecules, such as  $[\text{Ln}(\text{L})_3(\text{solvent})_2]$ -type complexes where only (solvent) is varied as one would expect these to have similar Raman and QTM regimes.<sup>108</sup> Furthermore,  $T_{\text{irrev}}$  is sometimes used which is the temperature at which field cooled (FC) and ZFC susceptibility data diverge.

$$\text{(Eq. 1)} \quad \tau^{-1} = \tau_{\text{QTM}}^{-1} + CT^n + \tau_0^{-1} e^{(-U_{\text{eff}}/k_B T)}$$

Relaxation times ( $\tau$ ) or rather relaxation rates ( $\tau^{-1}$ ) extracted from AC susceptibility and DC magnetization decay experiments can be fitted to Eq. 1 to extract  $U_{\text{eff}}$  and other terms; where  $T$  is temperature (K),  $k_B$  is Boltzmann’s constant,  $\tau_{\text{QTM}}^{-1}$  is the relaxation rate ( $\text{s}^{-1}$ ) in the QTM regime,  $C$  and  $n$  are empirical terms relating to two-phonon Raman relaxation, and  $\tau_0^{-1}$  is the attempt rate which is the time scale on which relaxation events occur for a given material. It is important to note that all processes are potentially in action (QTM, Raman, Orbach) at all temperatures. An example plot is shown in Figure 5a which depicts a graph of  $\ln(\tau)$  vs  $T^{-1}$  for a

fictitious SMM. For a real experiment, this data is extracted from frequency and temperature dependent AC susceptibility measurements, and DC magnetization decays, and the reader is directed to other works for a more detailed description of data collection and workup.<sup>17</sup> Figure 5b shows a hypothetical hysteresis plot. During the measurement of a single hysteresis loop the magnetization of the sample is recorded at a fixed temperature against a swept magnetic field which is either parallel ( $+H_{\text{ext}}$ ) or antiparallel ( $-H_{\text{ext}}$ ) with respect to the lab-frame z-axis. The magnetization in each opposing sweep direction should be symmetrical, but the value of  $|M / M_{\text{sat}}|$  at a given value of  $H_{\text{ext}}$  depends upon the magnetic history (hence hysteresis) of the sample. Precipitous drops in magnetization (green line) are ascribed to QTM.  $\Delta H$  between  $H_{\text{ext}} = 0$  and the field at which  $|M / M_{\text{sat}}|$  reaches zero is the coercive field, denoted by the dashed arrow and line.

At high temperatures where the Orbach process dominates, relaxation is governed by the rate of transition (and hence separation) between the KDs, and thus the strength of the crystal field is important. At extremely low temperatures ( $\sim 2$  K) QTM is usually dominant, and the rate is effectively governed by the transverse anisotropy which bridges  $\pm m_J$  states and thus is influenced by the off-axis contributions to the crystal field, along with hyperfine interactions and transverse (including dipolar) magnetic fields. In the presence of stray fields this applies for both Kramers and non-Kramers ions though it is worth noting that these factors generally cannot explain the entirety of zero-field relaxation even at 2 K.<sup>73</sup> The intervening temperature range is less understood as the terms  $C$  and  $n$  are empirically derived from the experimental data where the theoretically-predicted values are obtained on the basis of vast approximations.<sup>109</sup> Experimental values of  $n$  typically range from  $\sim 1$  up to  $\sim 8$ , and thus the temperature dependence in the Raman regime differs enormously between different molecules. In the following sections an account is provided through select examples of how synthetic chemistry has afforded control over, or at least significant insight into, disfavouring the QTM relaxation mechanism, and how values of  $U_{\text{eff}}$  approaching, and breaking past 1,000 K ( $695 \text{ cm}^{-1}$ ) have now been achieved. These developments have led to an understanding of design strategies for molecules where  $n$  is  $\sim 1$  to  $\sim 2$  and thus display very slow relaxation right up to  $\tau_{\text{switch}}$  where the Orbach mechanism becomes dominant. A deeper understanding of the electronic structure in SMMs requires recourse to more specialised techniques and a multi-disciplinary approach, as typically modelling magnetization data alone does not necessarily provide sufficient insight towards further strategies for improvement.<sup>110-113</sup>

## Discussion

### *High symmetry or bust?*

High-symmetry is an essential requirement for non-Kramers ions (e.g.  $\text{Tb}^{3+}$ ,  $\text{Ho}^{3+}$ ,  $\text{Tm}^{3+}$ ) to ensure a bistable ground state, while for Kramers ions in low symmetry (e.g.  $\text{Dy}^{3+}$ ,  $\text{Er}^{3+}$ ,  $\text{Yb}^{3+}$ ) QTM is still formally forbidden between degenerate KDs in the strict absence of any external field. However, this is unrealistic to achieve experimentally, as even the spin on distant neighbouring molecules will induce a small splitting between formally degenerate  $\pm m_J$  states, allowing QTM.<sup>17</sup> One approach to obviating this issue is to simply make the CF splitting substantially larger than the energy available to the system at a given temperature and take advantage of the fact that certain symmetries suppress specific types of CF transition.<sup>17</sup> As mentioned above, ligand disposition will effect whether a molecule has easy-axis anisotropy, a requisite for SMM behaviour, or instead easy-plane anisotropy. Two early SMMs by Wang and Gao both feature Kramers ions in formally low point group symmetry are  $[\text{Dy}(\text{acac})_3(\text{OH}_2)_2]$  (**3**,  $\text{acac} = \{\text{CH}(\text{CMeO})_2\}$ ),<sup>114</sup> and  $[\text{Er}(\text{COT})(\text{Cp}^*)]$  (**4-Er**,  $\text{COT} = \{\text{C}_8\text{H}_8\}$ ;  $\text{Cp}^* = \{\text{C}_5\text{Me}_5\}$ ),<sup>115</sup>

shown in Figure 6. Complex **3** is 8-coordinate with three acac ligands and two bound water molecules; the inequivalence in donor atoms makes it formally low symmetry and it should not be described using high symmetry point groups, however its coordination environment considering just the O atoms approximates a square antiprism.

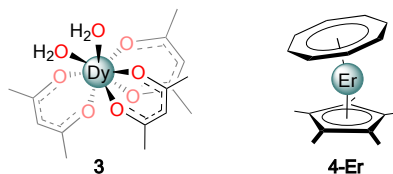


**Figure 6.** a)  $[\text{Dy}(\text{acac})_3(\text{OH}_2)_2]$  (**3**); b)  $[\text{Er}(\text{COT})(\text{Cp}^*)]$  (**4-Er**). A H-bonded  $\text{H}_2\text{O}$  and  $\text{EtOH}$  have been omitted from **3**.  $\text{acac} = \{\text{CH}(\text{CMeO})_2\}$ ,  $\text{COT} = \{\text{C}_8\text{H}_8\}$ ,  $\text{Cp}^* = \{\text{C}_5\text{Me}_5\}$ .

Complex **3** has a modest  $U_{\text{eff}}$  of  $46 \text{ cm}^{-1}$ , and shows only butterfly-shaped hysteresis even at temperatures below 2 K. Magnetometry measurements of both spin-dilute (1:20 Dy:Y doping), and pure Dy systems at  $\sim 0.5 \text{ K}$  showed that the reduction of dipolar interactions did not change the hysteresis profile which was still completely closed at zero-field.<sup>114</sup> The calculated gap between the ground KD ( $m_J = \pm 13/2$ ) and the 1<sup>st</sup> excited KD of  $28 \text{ cm}^{-1}$  is somewhat close to the experimentally observed  $U_{\text{eff}}$ , suggesting **3** relaxes *via* this state at high temperatures. Complex **4-Er** was the earliest organometallic Ln SMM and formally features  $C_s$  symmetry.<sup>115</sup> **4-Er** shows two  $U_{\text{eff}}$  barriers ( $137 \text{ cm}^{-1}$  and  $225 \text{ cm}^{-1}$ ), indicative of multiple relaxation processes occurring in the Orbach regime, which the authors attributed to two different crystallographically observed conformers of the molecules. In common with **3**, hysteresis loops for **4-Er** are butterfly-shaped at all temperatures, and thus rapid QTM is operant though  $T_H \approx 4 \text{ K}$  in this instance.<sup>114,115</sup> Despite both molecules possessing low formal symmetry, the favourable ligand arrangements and strong ligand field ensured that for both the ground-state has easy-axis anisotropy and thus they both have a barrier to their magnetic reversal. However, symmetry can be important for obviating zero-field relaxation even in Kramers ions,<sup>17</sup> and thus both have butterfly-shaped hysteresis profiles. This is further demonstrated upon moving to higher formal symmetry molecules such as in the  $[\text{Er}(\text{COT})_2]^-$  anion which has a similar ligand set to **4-Er** (*vide infra*). The **4-Ln** (Ln = Tb, Dy, Ho, Tm) analogues of **4-Er** were subsequently synthesized,<sup>116</sup> which allowed similar conclusions to be drawn. Long,<sup>117</sup> and also Chibotaru and Murugesu,<sup>118</sup> sought to see if the previously reported  $[\text{Er}(\text{COT})_2]^-$  anion,<sup>119</sup> which is related to **4-Er** but could display higher symmetry ( $D_{8h}$  or  $D_{8d}$ ), would engender better magnetic performance than **4-Er**. The complex was synthesized as:  $[\{\text{K}(18\text{-crown-6})\}(\mu\text{-}\eta^8\text{-}\eta^8\text{-COT})\text{Er}(\text{COT})]$  (**5-Er**)<sup>117,118</sup> which has the  $\text{K}^+$  coordinated  $\eta^8$ - to one of the COT rings; or  $[\text{K}(18\text{-crown-6})(\text{THF})_2][\text{Er}(\text{COT})_2]$  (**6-Er**, Figure 7) with a non-coordinated cation.<sup>117</sup>

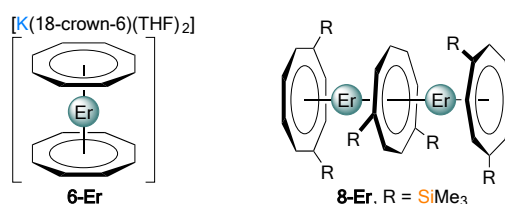


**Figure 7.** a)  $[K(18\text{-crown-6})(\text{THF})_2][\text{Er}(\text{COT})_2]$  (**6-Er**); b)  $[\text{Er}_2(\text{COT}'')_3]$  (**8-Er**).  $\text{COT} = \{\text{C}_8\text{H}_8\}$ ,  $\text{COT}'' = \{\text{C}_8\text{H}_6\text{-1,4-SiMe}_3\}$ .

Both **5-Er** and **6-Er** feature essentially, or perfectly, co-planar COT rings, and the large  $\pi$ -systems are perfectly disposed to stabilize an  $m_J = \pm 15/2$  ground state at  $\text{Er}^{3+}$  which requires an equatorial crystal field ( $U_{\text{eff}} = 147 \text{ cm}^{-1}$ ,<sup>117</sup> or  $199 \text{ cm}^{-1}$  for **5-Er**;<sup>118</sup> and  $150 \text{ cm}^{-1}$  for **6-Er**<sup>117</sup>). Both complexes **5-Er** and **6-Er** displayed butterfly-shaped hysteresis loops up to at least 10 K,<sup>117,118</sup> while the  $\text{Dy}^{3+}$  analogue (**5-Dy**) did not display hysteresis at any temperature.<sup>118</sup> Complex **5-Er** is not  $D_{8h}$ -symmetric due to a small degree of ring twisting ( $\sim 2.8^\circ$ ) and very slight  $\text{COT}_{\text{cent}} \cdots \text{Er} \cdots \text{COT}_{\text{cent}}$  bends ( $175.19^\circ$  and  $173.85^\circ$ ) and **6-Er** features essentially perfectly eclipsed rings,<sup>117</sup> and the bend angle is fixed at  $180^\circ$  by symmetry.<sup>117,118</sup> Despite these small differences in symmetry, both display superimposable magnetization data, thus low symmetry is not the sole cause of the QTM-like drop at zero-field. Spin-dilution of **6-Er** into a matrix composed of the diamagnetic  $\text{Y}^{3+}$  complex, **6-Y**, resulted in hysteresis loops that were open at zero-field up to at least 6 K, but  $T_{\text{H}}$  remained at 10 K.<sup>117</sup> The  $\{\text{Ln}(\text{COT})_n\}$  ( $n = 1$  or  $2$ ) moiety is a versatile building block,<sup>120,121</sup> and to that end several multi-decker complexes have been shown to act as SMMs. For example, mononuclear  $[\text{Li}(\text{DME})_3][\text{Er}(\text{COT}'')_2]$  (**7-Er**,  $\text{COT}'' = \{\text{C}_8\text{H}_6\text{-1,4-SiMe}_3\}$ )<sup>122</sup> ( $U_{\text{eff}} = 130 \text{ cm}^{-1}$ ,  $T_{\text{H}} = 8 \text{ K}$ ) can be transformed into the triple-decker  $[\text{Er}_2(\text{COT}'')_3]$  (**8-Er**), which features weak exchange coupling between  $\text{Er}^{3+}$  atoms.<sup>123</sup> Exchange constants cannot be readily measured for most  $\text{Ln}^{3+}$  complexes (where  $L \neq 0$ ), except for  $\text{Gd}^{3+}$  which has an orbital singlet ground state ( $^8\text{S}_{7/2}$ ,  $S = 7/2$ ,  $L = 0$ ,  $J = 7/2$ ) thus **8-Gd** was characterized by magnetometry and showed  $J = -0.448 \text{ cm}^{-1}$  ( $-\text{JS}_1\text{S}_2$  formalism).<sup>93</sup> When compared to mono-metallic **5-Er**, **6-Er**, or **7-Er**, complex **8-Er** showed an improved  $U_{\text{eff}}$  ( $219 \text{ cm}^{-1}$ ), and  $T_{\text{H}} = 12 \text{ K}$  (frozen dilute solutions gave  $T_{\text{H}} = 14 \text{ K}$ ), both demonstrate that the weakly exchange coupled complex has slightly better magnetic performance.<sup>117,118,122-124</sup>

The family of f-element sandwich complexes with carbocyclic rings larger than  $\text{Cp}^{\text{R}}$ , such as complexes **4-Er** to **8-Er** above, has been expanded to include  $\{\text{C}_9\text{H}_9\}^-$  in  $[\text{Er}(\text{COT})(\text{C}_9\text{H}_9)]$  (**9-Er**).<sup>125</sup> Due to its large size this could be expected to stabilize prolate ground states such as  $m_J = \pm 15/2$  for  $\text{Er}^{3+}$  similar to  $\{\text{COT}\}^{2-}$ . Indeed, complex **9-Er** has a relatively high  $U_{\text{eff}}$  of  $251 \text{ cm}^{-1}$  and *ab initio* calculations suggest the first few  $m_J$  states are ordered as  $\pm 15/2$ ,  $\pm 13/2$ ,  $\pm 1/2$ , where the  $m_J = \pm 1/2$  state lies at  $268 \text{ cm}^{-1}$  above the ground state which is in excellent agreement with the experimental  $U_{\text{eff}}$  and is the most likely relaxation pathway.<sup>125</sup> Even at 1.8 K **9-Er** displays butterfly-shaped hysteresis with no opening at zero-field, indicative of highly efficient QTM. This is likely a further indication that the design of  $\text{Er}^{3+}$  SMMs requires a good degree of local symmetry or exchange coupling, and shows that the design of such molecules is very difficult. An alternative avenue might be the exploitation of more symmetric divalent homoleptic *bis*- $\{\text{C}_9\text{H}_9\}$  complexes.<sup>126</sup> Structural and magnetic data for **4-Er** to **8-Er** is summarized in Table 1, unfortunately the disordered structure of **9-Er** does not permit detailed comparison to the *bis*- $\{\text{COT}\}$  complexes.<sup>125</sup>

**Table 1.** Structural and magnetic parameters for complexes **4-Er** to **8-Er**.

	$U_{\text{eff}} / \text{cm}^{-1}$	$T_{\text{H}} / \text{K}$	$L_{\text{cent}} \cdots \text{Er} \cdots \text{COT}_{\text{cent}} / ^{\circ} \dagger$
<b>4-Er</b>	137 / 225	~4	171.14(10)
<b>5-Er</b>	147 <sup>117</sup> or 199 <sup>118</sup>	10	178.62(15) <sup>117</sup> or 173.85(6) <sup>118</sup>
<b>6-Er</b>	150	10	180
<b>7-Er</b>	130	8	176.45(5)
<b>8-Er</b>	219	12	178.24(10) <sup>‡</sup>

<sup>†</sup> L is either Cp\*, or a COT ligand. <sup>‡</sup> Er...COT...Er angle = 175.65(11) °

An understanding of the orientation of the anisotropy axis of Ln complexes, as defined by the ligand field, is essential for the rationalization of magnetic properties and for guiding future synthetic targets. Indeed, the realization that the *bis*-{COT} framework does not provide an axial ligand field was essential to explaining the properties of the **5-Ln** complexes (Ln = Er<sup>3+</sup> and Dy<sup>3+</sup>). The development of *ab initio* electronic structure methods that could predict the anisotropy axis in real molecules has helped in this respect.<sup>43,89,127,128</sup> As most low-symmetry Dy<sup>3+</sup> complexes possess a strongly axial ground-state  $m_J = \pm 15/2$ , approximations can be made instead for this ion, and an alternate model was developed using an electrostatic optimization methodology, which requires only an X-ray diffraction structure as input.<sup>97,129</sup>

#### Preventing QTM through exchange interactions

Whilst high symmetry can help reduce QTM, nearly all high-performing SMMs still display a precipitous drop of magnetization at zero-field due to QTM. One elegant approach to suppress QTM and hence resolve the butterfly-shaped hysteresis issue is to use strategies from the d-block, and synthesize molecules that utilize ferromagnetic or antiferromagnetic exchange interactions leading to exchange bias.<sup>130</sup> The *tris*-[1]ferrocenophane (Fc = {Fe(C<sub>5</sub>H<sub>4</sub>)<sub>2</sub>}<sup>2-</sup>) complexes [Li(THF)<sub>4</sub>][Ln(Fc)<sub>3</sub>{Li(THF)}<sub>2</sub>] (**10-Ln**, Ln = Tb, Dy, Ho) have approximate trigonal prismatic symmetry about the metal and exemplify these complexities very well. They also show modest  $U_{\text{eff}}$  values in zero-field (Ln = Tb, 274 cm<sup>-1</sup>; Dy, 110 cm<sup>-1</sup>; Ho, two processes 110 cm<sup>-1</sup> and 131 cm<sup>-1</sup>), and show butterfly-shaped hysteresis ( $T_{\text{H}} \sim 4$  K), except for the Ho<sup>3+</sup> congener which showed closed loops even at 2 K.<sup>131-133</sup> Two units of monomeric **10-Dy** can be bridged by a third Dy<sup>3+</sup> to form centrosymmetric [Li(THF)<sub>3</sub>]<sub>2</sub>(μ-Cl)[{Dy(Fc)<sub>3</sub>]<sub>2</sub>(μ<sub>6</sub>-Dy)] (**11-Dy**) which shows two  $U_{\text{eff}}$  values (261 cm<sup>-1</sup> and 268 cm<sup>-1</sup>) due to the two Dy<sup>3+</sup> environments, and  $T_{\text{H}} = 5$  K with open loops even at zero-field.<sup>134</sup> Susceptibility measurements suggest ferromagnetic exchange is behind the improved performance relative to **10-Dy**, though further study is needed to determine if dipolar (through space) coupling,<sup>135,136</sup> or superexchange (mediated by the electrons on intervening atoms) dominates.<sup>137</sup>

Direct Ln...Ln exchange is usually small due to the poor radial extension of their valence orbitals ( $|J| < 1$  cm<sup>-1</sup> typically),<sup>138,139</sup> and superexchange pathways are correspondingly limited for the same reason.<sup>140-143</sup> For example, in a series of pnictogen-bridged trimetallic cyclopentadienide complexes,<sup>144-146</sup> the magnetic behaviour is best described as a series of non-interacting SMMs with axial crystal fields. Indeed, even relatively small charge diffuse bridges can be inefficient at mediating superexchange, while also keeping Ln<sup>3+</sup> ions too far apart for significant direct exchange.<sup>147</sup> It should be noted that in rare instances, Ln...Ln exchange interactions

can be ferromagnetic rather than the much more common anti-ferromagnetic.<sup>148-151</sup> This can help to suppress QTM and appears to be related to having the anisotropy axis on each metal coincident, or close to, the Ln...Ln vector.

Direct strong coupling with spin-active moieties such as  $N_2^{3-}$  radicals,<sup>152-155</sup> or organic radicals,<sup>156-159</sup> are an alternative that has been shown to engender large antiferromagnetic coupling between the Ln and the radical spin. As long as the antiferromagnetic Ln...radical exchange coupling is stronger than any Ln...Ln coupling, all the Ln spins can potentially orient in the same direction, and the whole system can act as one giant spin that is harder to flip than each spin alone. Several complexes prepared by Evans and Long [K(18-crown-6)(THF)<sub>2</sub>][{Ln(N'')<sub>2</sub>(THF)}<sub>2</sub>(μ-N<sub>2</sub><sup>3-</sup>)] (**12-Ln**, Ln = Gd, Tb, Dy, Ho, Er; N'' = {N(SiMe<sub>3</sub>)<sub>2</sub>}),<sup>152</sup> and also the closely related [K(2.2.2-crypt)][{Ln(Cp<sup>tet</sup>)<sub>2</sub>(THF)<sub>n</sub>}(μ-N<sub>2</sub><sup>3-</sup>)] (**13-Ln**, n = 1, Ln = Gd, Tb, Dy; **14-Ln**, Ln = Tb, Dy, n = 0; Cp<sup>tet</sup> = {C<sub>5</sub>Me<sub>4</sub>H}) by Demir and Long,<sup>154</sup> effectively demonstrate the effects of strong exchange coupling towards generating large coercive fields. Complexes **12-Tb** and **14-Tb** are shown in Figure 8.

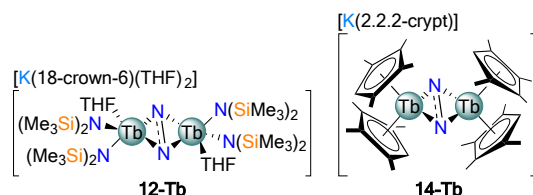


**Figure 8.** a) [K(18-crown-6)(THF)<sub>2</sub>][{Tb(N'')<sub>2</sub>(THF)}<sub>2</sub>(μ-N<sub>2</sub><sup>3-</sup>)] (**12-Tb**); b) [K(2.2.2-crypt)][{Ln(Cp<sup>tet</sup>)<sub>2</sub>(μ-N<sub>2</sub><sup>3-</sup>)] (**14-Tb**). N'' = {N(SiMe<sub>3</sub>)<sub>2</sub>}, Cp<sup>tet</sup> = {C<sub>5</sub>Me<sub>4</sub>H}.

Complexes **12-Ln**, **13-Ln** and **14-Ln** all feature an  $N_2^{3-}$  radical bridging ligand, the SOMO of which is comprised of a diffuse  $\pi^*$  orbital that lies perpendicular to the Ln<sub>2</sub>N<sub>2</sub> plane.<sup>155</sup> The Gd–N<sub>2</sub> coupling constant was measured for **12-Gd** ( $J = -27 \text{ cm}^{-1}$ ), and **13-Gd** ( $J = -20 \text{ cm}^{-1}$ ).<sup>153,154</sup> By virtue of the strong anti-ferromagnetic coupling between metal and radical in **12-Ln**, the spin on the two metals is forced to be co-parallel and leads to an effective giant spin. Whilst complexes **12-Tb** and **12-Dy** displayed only modest  $U_{\text{eff}}$  values (227  $\text{cm}^{-1}$  and 123  $\text{cm}^{-1}$ , respectively) they both showed giant coercivity and essentially no zero-field step in hysteresis measurements, high  $T_{B2}$  (14 K for **12-Tb**) and record-setting  $T_H$  values (14 K and 8 K, respectively).<sup>152</sup> A theoretical study has proposed values of  $J$  for the non-Gd complexes, and that multiples of these values correlate with the experimentally determined  $U_{\text{eff}}$  values in the **12-Ln** series.<sup>160</sup> Complexes **13-Ln** and **14-Ln** represent a further improvement to this strategy, where the *bis*-{CpMe<sub>4</sub>H} ligand framework engenders a similar axial field to *bis*-{N''}, thus  $U_{\text{eff}}$  values are similar (**13-Tb**, 242  $\text{cm}^{-1}$ ; **13-Dy**, 110  $\text{cm}^{-1}$ ; *c.f.* **12-Tb**, 227  $\text{cm}^{-1}$ ); furthermore the THF moieties in **13-Ln** are easily displaced to afford **14-Tb** and **14-Dy**.<sup>154</sup> In **14-Tb** the loss of THF led to a significant improvement in the anisotropy barrier, though two thermally activated relaxation processes were observed ( $U_{\text{eff}1} = 276 \text{ cm}^{-1}$ ,  $U_{\text{eff}2} = 564 \text{ cm}^{-1}$ ); along with a remarkably high  $T_{B2}$  (20 K), a giant coercive field of 7.9 T at 10 K, and  $T_H = 30 \text{ K}$ . For **14-Dy** there was almost no effect on the barrier ( $U_{\text{eff}} = 108 \text{ cm}^{-1}$ ) upon removal of THF *c.f.* **13-Dy**; however, while **13-Dy** displayed no remnant magnetization at any temperature above 2 K, **14-Dy** showed open hysteresis loops up to 8 K.<sup>154</sup> These data are summarised in Table 2.

**Table 2.** Magnetic parameters for complexes **12-Tb** to **14-Tb** and **12-Dy** to **14-Dy**.

	<b>12-Tb</b>	<b>12-Dy</b>	<b>13-Tb</b>	<b>13-Dy</b>	<b>14-Tb</b>	<b>14-Dy</b>
$U_{\text{eff}} / \text{cm}^{-1}$	227	123	242	110	276 / 564	108
$T_{\text{B}_2} / \text{K}$	13.9	6.7	-	-	20	-
$T_{\text{H}} / \text{K}$	14	8	15	-	30	8

Nitrogenous heterocycles can also be used to couple Ln centers that have easily displaced ligands such as the weakly coordinating anion  $\{\text{BPh}_4\}^-$  in  $[\text{Dy}(\text{Cp}^*)_2(\text{BPh}_4)]$  (**15-Dy**).<sup>156,161,162</sup> Complex **15-Dy**, and related  $[\text{Dy}(\text{Cp}^R)_2(\text{X})]$  ( $\text{Cp}^R$  = substituted Cp, X = equatorial ligand) complexes, often show  $U_{\text{eff}}$  values of 150 – 600  $\text{cm}^{-1}$  as they have strong axial ligand fields with correspondingly large KD separations; however, they invariably have butterfly-shaped hysteresis profiles as the transverse anisotropy induced by the co-ligands allows rapid QTM-like relaxation at zero-field, even for Kramers ion  $\text{Dy}^{3+}$ .<sup>48,142,143,163-168</sup> The radical bridged complexes in Figure 9,  $[\{\text{Dy}(\text{Cp}^*)_2\}_2(\text{bpym})][\text{BPh}_4]$  (**16-Dy**, bpym = 2,2'-bipyrimidine),<sup>156</sup>  $[\{\text{Dy}(\text{Cp}^*)_2\}_2(\text{tppz})][\text{BPh}_4]$  (**17-Dy**, tppz = 2,3,5,6-tetra(2-pyridyl)pyrazine),<sup>169</sup> and  $[\{\text{Dy}(\text{Cp}^*)_2\}_3(\text{HAN})]$  (**18-Dy**, HAN = hexaazatrinaphthylene),<sup>158</sup> have significantly smaller  $U_{\text{eff}}$  values (**16-Dy**, 88  $\text{cm}^{-1}$ ; **17-Dy**, 36  $\text{cm}^{-1}$ ; **18-Dy**, 51  $\text{cm}^{-1}$  respectively) than many  $[\text{Dy}(\text{Cp}^R)_2(\text{X})]$  complexes,<sup>163,164</sup> but show open hysteresis loops at zero-field and remnant magnetization ( $T_{\text{H}} = 6.5 \text{ K}$ , 3.25 K, and 3.5 K respectively). The reduced analogue of **17-Dy**,  $[\text{K}(2.2.2\text{-crypt})][\{\text{Dy}(\text{Cp}^*)_2\}_2(\text{tppz})]$  (**19-Dy**) features a different distribution of spin-density at the  $\text{tppz}^{3-}$  bridge to **17-Dy**, and neither **19-Dy** or the Tb analogue **19-Tb** show either zero-field or in-field slow relaxation dynamics.<sup>169</sup> This organic linker strategy allows for significant scope in controlling nuclearity. For all radical-bridged systems, variation of radical ligand oxidation state allows total spin, and strength of the exchange interaction to be mediated through chemical design.<sup>170</sup>

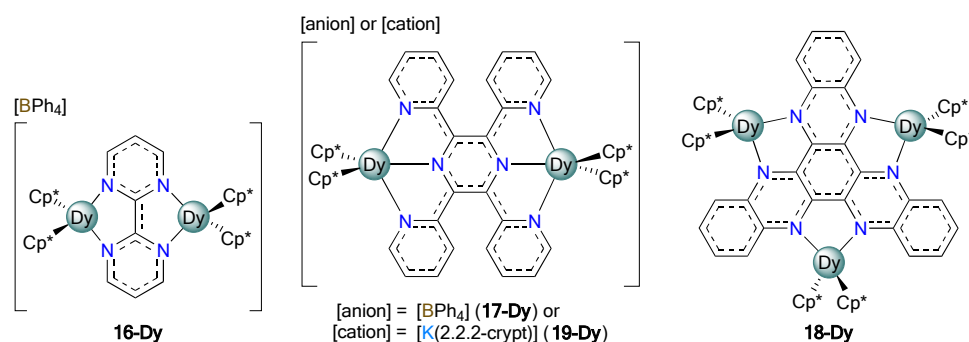
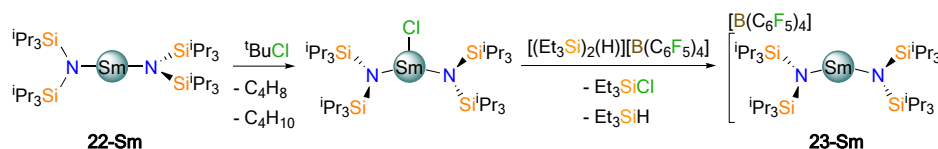


**Figure 9.** a)  $[\{\text{Dy}(\text{Cp}^*)_2\}_2(\text{bpym})][\text{BPh}_4]$  (**16-Dy**); b)  $[\{\text{Dy}(\text{Cp}^*)_2\}_2(\text{tppz})][\text{BPh}_4]$  (**17-Dy**) or  $[\text{K}(2.2.2\text{-crypt})][\{\text{Dy}(\text{Cp}^*)_2\}_2(\text{tppz})]$  (**19-Dy**); d)  $[\{\text{Dy}(\text{Cp}^*)_2\}_3(\text{HAN})]$  (**18-Dy**). bpym = 2,2'-bipyrimidine, tppz = 2,3,5,6-tetra(2-pyridyl)pyrazine, HAN = hexaazatrinaphthylene.

#### The axial ligand field approach

Most of the Ln SMMs discussed above have first excited KDs high enough above the ground state that there should not be phonons available to promote excitations at very low temperatures. Other effects such as transverse anisotropy induced by co-ligands that are not placed with precise point group symmetry are thus

important. There has thus been a drive to increase  $U_{\text{eff}}$  dramatically by maximizing the spatial axiality of ligands while minimizing equatorial contributions, reducing the off-axis terms as much as possible.<sup>171,172</sup> A larger  $U_{\text{eff}}$  will increase  $\tau$  at least in the high-temperature regime. Proposals for high-barrier SMMs that are also synthetically realistic is of paramount importance. *In silico* predictions by Ungur and Chibotaru for isolated  $[\text{Dy}=\text{O}]^+$ , and linear  $[\text{F}-\text{Dy}-\text{F}]^+$  clearly show that they possess the desired ordering of pure  $m_J$  states and massive separation of the first two KDs ( $\sim 490 - 700 \text{ cm}^{-1}$ ),<sup>63,64</sup> however they are not isolable molecules outside of matrix isolation experiments.<sup>173</sup> It should be noted that while the ordering of  $m_J$  states in  $\text{Dy}^{3+}$  from most-magnetic to least is ensured with a strong axial ligand field, as  $m_J = \pm 15/2$  is oblate and  $m_J = \pm 1/2$  is prolate,<sup>56</sup> the opposite is true for  $\text{Er}^{3+}$  where instead a strong equatorial ligand field stabilizes  $m_J = \pm 15/2$  and destabilizes  $m_J = \pm 1/2$ . Thus complexes such as pyramidal  $[\text{Er}(\text{N}^{\text{i}})_3]$  (**20-Er**) which has crystallographically imposed  $C_{3v}$  symmetry, or  $[\text{Er}(\text{HNDipp})_3(\text{THF})_2]$  (**21-Er**,  $\text{Dipp} = \{\text{C}_6\text{H}_3-2,6\text{-iPr}\}$ ) where the anionic charge is concentrated about the equator, both present modest  $U_{\text{eff}}$  values ( $85 \text{ cm}^{-1}$ , **20-Er**;  $17.4 \text{ cm}^{-1}$ , **21-Er**), though both show butterfly-shaped hysteresis at 1.9 K.<sup>174</sup> Derivatives of **20-Er** with axial ligand fields have been studied in depth, and even weak axial donors result in diminished  $U_{\text{eff}}$  values.<sup>175,176</sup> The large  $\pi$ -cloud in  $\{\text{COT}\}^{2-}$  offers a more equatorial ligand field in **4-Er** to **8-Er**, than it does axial, hence their good  $U_{\text{eff}}$  values.<sup>117,118,122-124</sup>



**Scheme 1.** Reaction scheme detailing the synthesis of  $[\text{Sm}\{\text{N}(\text{Si}^i\text{Pr}_3)_2\}_2][\text{B}(\text{C}_6\text{F}_5)_4]$  (**23-Sm**) from  $[\text{Sm}\{\text{N}(\text{Si}^i\text{Pr}_3)_2\}_2]$  (**22-Sm**),  $\text{tBuCl}$ , and  $[(\text{Et}_3\text{Si})_2(\text{H})][\text{B}(\text{C}_6\text{F}_5)_4]$ .

A series of two-coordinate  $\text{Ln}^{2+}$  silylamide complexes,  $[\text{Ln}\{\text{N}(\text{Si}^i\text{Pr}_3)_2\}_2]$  (**22-Ln**,  $\text{Ln} = \text{Eu}, \text{Sm}, \text{Tm}, \text{Yb}$ ) was reported (Scheme 1) which show nearly ideal geometries for a proposed axial  $\text{Dy}^{3+}$  SMM (e.g.  $\text{N}-\text{Sm}-\text{N} = 175.52(18)^\circ$ ).<sup>177,178</sup> Calculations on a cationic  $\text{Dy}^{3+}$  analogue of **22-Sm**,  $[\text{Dy}\{\text{N}(\text{Si}^i\text{Pr}_3)_2\}_2]^+$ , suggested it could have a  $U_{\text{eff}} > 1,800 \text{ cm}^{-1}$ , and further work showed that other formally 2-coordinate  $\text{Dy}^{3+}$  complexes that represented realistic, albeit challenging, synthetic targets with stronger donors could have even higher  $U_{\text{eff}}$  values.<sup>100</sup> Subsequently,  $[\text{Ln}\{\text{N}(\text{Si}^i\text{Pr}_3)_2\}_2][\text{B}(\text{C}_6\text{F}_5)_4]$  (**23-Ln**;  $\text{Ln} = \text{Sm}, \text{Tm}, \text{Yb}$ ; Scheme 1) were reported as borate salts, which were derived from oxidation of the **22-Ln** complexes with halide sources,<sup>179</sup> followed by halide abstraction using the super-electrophile  $[(\text{Et}_3\text{Si})_2(\text{H})][\text{B}(\text{C}_6\text{F}_5)_4]$  (Scheme 1).<sup>180</sup> Each  $\text{Ln}^{3+}$  ion in **23-Ln** is formally two-coordinate, though there is significant deviation from linearity (e.g. for **23-Sm**  $\text{N}-\text{Sm}-\text{N} = 131.02(8)^\circ$ ). Given the only modest dependence of  $U_{\text{eff}}$  on  $\text{L}-\text{Dy}-\text{L}$  in systems without equatorial Lewis-Base donors, hypothetical **23-Dy** could still have a barrier larger than  $1,400 \text{ cm}^{-1}$ .<sup>100</sup>

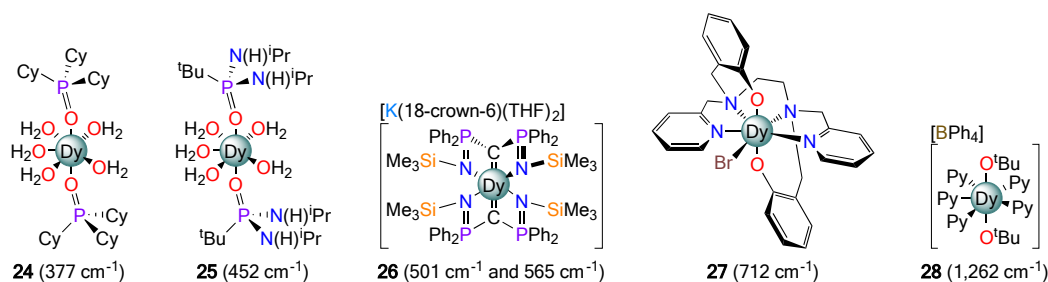


**Figure 10.** Complexes **24–28** (values in brackets refer to the  $U_{\text{eff}}$ ) are five molecules that successively raised the  $U_{\text{eff}}$  record for Dy<sup>3+</sup> SMMs from 377 cm<sup>-1</sup> to 1,262 cm<sup>-1</sup> in one year (2016), while also finally demonstrating Dy-based SMMs with superior  $U_{\text{eff}}$  values to {TbPc}-based SMMs. Hydrogen bonded halides and additional equivalents of phosphine-oxide have been omitted from both **24** and **25** to highlight the five equatorial H<sub>2</sub>O moieties, and the axial ligands only. For simplicity, complex **26** is drawn as one extreme of its various resonance structures.

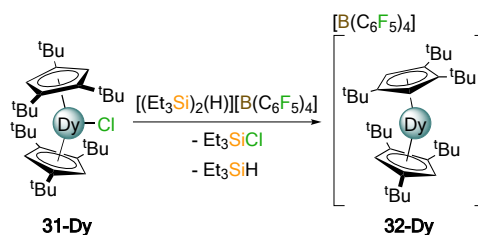
Shortly after the disclosure of **22-Sm**, a number of SMMs (**24–28**, Figure 10 shows some examples) were reported with phenomenal  $U_{\text{eff}}$  barriers using Dy<sup>3+</sup>.<sup>181–185</sup> Although complexes **24–26** do not represent the largest values of  $U_{\text{eff}}$  (377 cm<sup>-1</sup>, 452 cm<sup>-1</sup>, and 501 cm<sup>-1</sup> / 565 cm<sup>-1</sup>) they demonstrate a guided design approach to synthetically accessible Dy<sup>3+</sup> SMMs: 1) strong axial ligand fields, with equatorial interactions weakened as much as possible; 2) equatorial ligands are disposed with fairly high symmetry thus minimizing transverse anisotropies. All (**24–28**) have a ground  $m_J = \pm 15/2$  with reasonably pure first excited KDs, with **26** and **28** possessing second excited states comprised of >96%  $m_J = \pm 11/2$ . For example, in complex **26** the first 3 KDs are ordered  $m_J = \pm 15/2, \pm 13/2, \pm 11/2$  and are quantized along the C=Dy=C axis to within a few degrees.<sup>183</sup> Complex **28**, a cationic *bis*-alkoxide [Dy(O<sup>t</sup>Bu)<sub>2</sub>(Py)<sub>5</sub>][BPh<sub>4</sub>] features an extremely large barrier ( $U_{\text{eff}} = 1,262$  cm<sup>-1</sup>) by virtue of the two strong axial alkoxide donors and comparatively weak equatorial pyridine donors. Despite this large barrier, **28** displays butterfly-shaped hysteresis ( $T_{\text{H}} = 4$  K), though  $T_{\text{B}1} = 14$  K. An exhaustive study of an extended family of pentagonal bipyramidal complexes related to **28**, where the axial and equatorial ligands were systematically changed, showed a good correlation between  $U_{\text{eff}}$  and  $T_{\text{H}}$  within this structurally analogous series of complexes.<sup>186</sup> Such studies are unfortunately rare, and should be considered essential to further progress. The exceptional barriers of these complexes have raised interesting questions regarding the fundamental assumptions about how SMMs lose magnetization. Since high barriers alone do not preclude alternative relaxation mechanisms, a better understanding of the relationship between structure and relaxation mechanisms is needed, and in particular how ligand vibrations interact with the magnetic moments.<sup>73,105,108,113,187</sup>

#### High-temperature remanence in Ln metallocene(ium)s

*Ab initio* calculations suggest that an isolated [Dy(Cp<sup>\*</sup>)<sub>2</sub>]<sup>+</sup> cation, featuring a Cp<sub>cent</sub>⋯Dy⋯Cp<sub>cent</sub> angle of just 136° could possess a  $U_{\text{eff}}$  of over 1,000 cm<sup>-1</sup>, and extremely small transverse anisotropy up to at least the 3<sup>rd</sup> or 4<sup>th</sup> KD, this could result in an SMM with high-temperature magnetic remanence.<sup>164</sup> Unfortunately, the (relatively) small size of the Cp<sup>\*</sup> ligand precludes the isolation of such a species with Ln<sup>3+</sup> ions, and even with smaller metals such as Sc<sup>3+</sup>.<sup>157,161,188–190</sup> Numerous studies on real molecules have demonstrated that the crystal field in {Dy(Cp<sup>R</sup>)<sub>2</sub>}-containing complexes is dominated by the Cp<sup>R</sup>–Dy–Cp<sup>R</sup> motif, and thus such species are desirable targets.<sup>191,192</sup> Two complexes have exemplified the difficulty in synthesizing isolated [Dy(Cp<sup>\*</sup>)<sub>2</sub>]<sup>+</sup>

cations due to their extreme electrophilicity, and also on the sensitivity of relaxation mechanisms to subtle structural changes.<sup>193,194</sup> The centrosymmetric complex  $[\{\text{Dy}(\text{Cp}^*)_2\}_2\{\mu\text{-AlMe}_3\text{NEt}_3\}_2][\text{Al}\{\text{OC}(\text{CF}_3)_3\}_4]_2$  (**29-Dy**) features neutral bridging ligands ( $\text{AlMe}_3\text{NEt}_3$ ) bound only through agostic-type  $\text{C-H}\cdots\text{Dy}$  or  $\text{C}\cdots\text{Dy}$  interactions;<sup>193</sup> and  $[\{\text{Dy}(\text{Cp}^*)_2\}_2(\mu\text{-BPh}_4)][\text{Al}\{\text{OC}(\text{CF}_3)_3\}_4]$  (**30-Dy**) which is bridged by formally anionic  $\{\text{BPh}_4\}^-$ .<sup>194</sup> Complexes **29-Dy** and **30-Dy** are almost identical metrically by inspection of their respective  $\text{Cp}_{\text{cent}}\cdots\text{Dy}$  distances (**29-Dy**, 2.348(3) Å and 2.388(3) Å vs **30-Dy**, range: 2.357(2) Å to 2.359(2) Å) and  $\text{Cp}_{\text{cent}}\cdots\text{Dy}\cdots\text{Cp}_{\text{cent}}$  angles (**29-Dy**, 138.03° vs **30-Dy**, 134.7° and 135.4°), and the range of  $\text{Dy-C}_{\text{bridge}}$  distances differ by less than 0.15 Å in total. Coincident with these minimal structural changes, their electronic structures from *ab initio* calculations are similar for the first 4 KDs ( $m_J = \pm 15/2, \pm 13/2, \pm 11/2, \pm 9/2$ ). However, for **30-Dy** the main anisotropy axis of the 5<sup>th</sup> KD (668  $\text{cm}^{-1}$  avg. across both metals) lies perpendicular to the  $\{\text{Dy}(\text{Cp}^*)_2\}$  axis and is highly mixed,<sup>194</sup> whereas this occurs at the 6<sup>th</sup> KD ( $E = 842 \text{ cm}^{-1}$ ) for **29-Dy** which is coincident with the experimental  $U_{\text{eff}}$  (860  $\text{cm}^{-1}$ ).<sup>193</sup> For **30-Dy** the  $U_{\text{eff}}$  (340  $\text{cm}^{-1}$ ) is close to the average values for both the 2<sup>nd</sup> KD (246  $\text{cm}^{-1}$ ) and 3<sup>rd</sup> KD (460  $\text{cm}^{-1}$ ) between both metal sites. Both complexes display butterfly-shaped hysteresis profiles, and values of  $T_{\text{H}}$  (6.5 K, **30-Dy**; and 12 K, **29-Dy**) broadly agree with the differences in  $U_{\text{eff}}$ . Thus, it appears that the presence of a neutral vs anionic bridge is important.

Nief showed that the bulky alkylated  $\{\text{Cp}^{\text{ttt}}\}$  ligand ( $\text{Cp}^{\text{ttt}} = \{\text{C}_5\text{H}_2\text{-1,2,4-}^t\text{Bu}_3\}$ ) was capable of supporting monomeric  $[\text{Dy}(\text{Cp}^{\text{ttt}})_2(\text{X})]$  species ( $\text{X} = \text{Br}, \text{I}, \text{BH}_4$ ).<sup>195</sup> A modification using  $\text{DyCl}_3$  instead of  $\text{DyI}_3$ , afforded  $[\text{Dy}(\text{Cp}^{\text{ttt}})_2(\text{Cl})]$  (**31-Dy**, Figure 12).<sup>196</sup> As might be expected, **31-Dy** is a poor SMM ( $U_{\text{eff}} = 39 \text{ cm}^{-1}$ , with no hysteresis down to 2 K).<sup>197,198</sup> Separate works by Mills and Chilton,<sup>196</sup> and Layfield,<sup>198</sup> showed that anion abstraction strategy used to synthesize **23-Ln** (Scheme 1) worked with **31-Dy** to afford the first “dysprosocenium” cation,  $[\text{Dy}(\text{Cp}^{\text{ttt}})_2][\text{B}(\text{C}_6\text{F}_5)_4]$  (**32-Dy**, Scheme 2).<sup>196,198</sup> In complex **32-Dy** the two  $\text{Cp}^{\text{ttt}}$  ligands preclude close contact of the borate anion (nearest  $\text{Dy}\cdots\text{F} = 5.996(3) \text{ Å}$ ), are more axially-disposed than in the precursor (in cationic **32-Dy**,  $\text{Cp}_{\text{cent}}\cdots\text{Dy}\cdots\text{Cp}_{\text{cent}} = 152.56(7)^\circ$ ; *c.f.*  $146.67(7)^\circ$  in **31-Dy**), and are more tightly bound (in **32-Dy** mean  $\text{Cp}_{\text{cent}}\cdots\text{Dy} = 2.316(3) \text{ Å}$ ; *c.f.*  $2.413(3) \text{ Å}$  in **31-Dy**).<sup>196</sup> CASSCF-SO calculations on the electronic structure using the unoptimized X-ray diffraction structure showed the first six KDs were well-described by  $m_J = \pm 15/2, \pm 13/2, \pm 11/2, \pm 9/2, \pm 7/2, \pm 5/2$ , and are quantized along the  $\text{Cp}\cdots\text{Dy}\cdots\text{Cp}$  axis, whereas the two highest doublets are characterized by >5% mixing with other states and are oriented perpendicular to the principal axis.<sup>196</sup> AC susceptibility measurements gave  $U_{\text{eff}} = 1,223 \text{ cm}^{-1}$  (or  $1,277 \text{ cm}^{-1}$ ),<sup>196,198</sup> while  $T_{\text{B1}} = 38 \text{ K}$ ,  $T_{\text{B2}} = 53 \text{ K}$  and  $T_{\text{irrev}} = 60 \text{ K}$ . The large  $U_{\text{eff}}$  suggests that **32-Dy** relaxes *via* at least the 6<sup>th</sup> KD ( $1,278 \text{ cm}^{-1}$ ), and hysteresis measurements showed open loops ( $T_{\text{H}}$ ) up to 60 K at zero-field.<sup>196,198</sup> Interestingly, zero-field relaxation is almost entirely suppressed at low temperatures, with only a small step observed.<sup>196,198</sup> Fitting magnetization data to Eq. 1 at low temperature (23 to 50 K;  $\tau^{-1} = CT^n$ ) gave an unusually low exponent,  $n = 2.151$ .<sup>113,196,198</sup>



**Scheme 2.** The synthesis of  $[\text{Dy}(\text{Cp}^{\text{ttt}})_2][\text{B}(\text{C}_6\text{F}_5)_4]$  (**32-Dy**) from  $[\text{Dy}(\text{Cp}^{\text{ttt}})_2(\text{Cl})]$  (**31-Dy**) and  $[(\text{Et}_3\text{Si})_2(\text{H})][\text{B}(\text{C}_6\text{F}_5)_4]$ .  $\text{Cp}^{\text{ttt}} = \{\text{C}_5\text{H}_2\text{-}1,2,4\text{-tBu}_3\}$ .

An *ab initio* spin-dynamics study into the cation of **32-Dy** suggested that two ligand vibrational modes involving the C–H groups are key in mediating the first transition from  $m_J = \pm 15/2$  to  $\pm 13/2$  ( $489 \text{ cm}^{-1}$ ), and hence substitution of the H atoms could drastically alter the energy of these modes and take them off resonance with the first excitation.<sup>196</sup> New insights into the model system, **32-Dy**, have shown that this is an incomplete picture.<sup>113</sup> From a glance at Eq. 1, it should not be surprising that a low Raman exponent is absolutely essential for high-temperature SMMs as this mediates the relaxation rate up to  $\tau_{\text{switch}}$  when the much faster Orbach mechanism dominates, however the molecular features that define this constant are not immediately obvious. Combined experimental measurements and *ab initio* calculations have described the essential components that contribute to this relaxation regime as: 1) a large CF splitting ensures that only the ground KD is significantly populated, this is directly controllable *via* ligand choices leading to strong fields of appropriate geometry; 2) there should be only small magnetoelastic coupling, meaning that molecular vibrational modes (optical phonons) that influence the CF at Dy should be high in energy which can be achieved by using rigid ligands; 3) the optical phonon density of states (DOS) should not increase strongly with energy, *i.e.* having a large DOS of low-energy phonons that cannot bridge CF gaps should be acceptable, but the DOS of high-energy phonons which can bridge CF gaps should be as low as possible.<sup>73,113</sup> It is not immediately obvious how synthetic chemistry can control properties such as the DOS of optical and acoustic phonons, however extension of the **32-Ln** motif to the entire  $\text{Ln}^{3+}$  series has shown that low Raman exponents are a distinct feature of isolated  $[\text{Ln}(\text{Cp}^{\text{ttt}})_2]^+$  cations.<sup>199,200</sup> The rigid molecular structure increases the energy of intramolecular vibrational modes (optical phonons), and very weak intermolecular interactions by virtue of the anion-cation ion system which leads to large separations.

An elegant demonstration of the importance of symmetry in highly-axial complexes with non-Kramers ions is shown by cationic  $[\text{Ln}(\text{Cp}^{\text{iPr5}})_2][\text{B}(\text{C}_6\text{F}_5)_4]$  (**33-Ln**,  $\text{Ln} = \text{Tb}$  and  $\text{Dy}$ ;  $\text{Cp}^{\text{iPr5}} = \{\text{C}_5^{\text{iPr}}\text{Pr}_5\}$ ) complexes which feature  $\text{Ln}^{3+}$ , and neutral  $[\text{Ln}(\text{Cp}^{\text{iPr5}})_2]$  (**34-Ln**,  $\text{Ln} = \text{Tb}$  and  $\text{Dy}$ ) complexes with  $\text{Ln}^{2+}$  (Figure 11).<sup>201,202</sup> Complexes **34-Ln** are remarkable for being the first neutral linear 4f metallocenes for  $\text{Ln} \neq \text{Eu}$ ,  $\text{Yb}$  or  $\text{Sm}$ .<sup>203-206</sup> Both **33-Dy** and **34-Tb** have non-integer numbers of electrons in their valence shells (**34-Dy** is  $\text{Dy}^{3+}$ , therefore  $4f^9$ ; and divalent **34-Tb** features a  $4f^85d^1$  configuration) hence they are Kramers ions. Correspondingly, **33-Tb** and **34-Dy** are both non-Kramers ions with  $4f^8$  and  $4f^95d^1$  configurations respectively. Thus **34-Tb** could be viewed as a higher symmetry analogue of **33-Dy**. Non-Kramers **33-Tb** displayed essentially no hysteresis even at 2 K (in analogy to **32-Tb**),<sup>199</sup> and **34-Dy** exhibited butterfly-shaped hysteresis loops up to 75 K.<sup>202</sup> Rapid relaxation due to Raman and QTM processes precluded detailed analysis of the dynamic magnetization properties for **33-Tb**, while a  $U_{\text{eff}}$  ( $37 \text{ cm}^{-1}$ ) could only be determined for **34-Dy** in an applied field to suppress QTM. The reader should note the enormous disparity between the high  $T_{\text{H}}$  (75 K, though butterfly-shaped) and small  $U_{\text{eff}}$  in **34-Dy**.

Conversely, the Kramers ion-containing **33-Dy** and **34-Tb** show large  $U_{\text{eff}}$  values (1,334  $\text{cm}^{-1}$  and 1,205  $\text{cm}^{-1}$ ) both approaching or surpassing that of **32-Dy**. They display  $T_{\text{H}}$  values (66 K and 55 K, respectively) that approach that of the boiling point of liquid nitrogen (77 K,  $-196^{\circ}\text{C}$ ), widely regarded as a floor in performance for device-usage; and high  $T_{\text{B}2}$  values of 56 K and 52 K, respectively.<sup>201,202</sup> The much larger power-law temperature dependence of Raman relaxation for **34-Tb** ( $n = 8.69$ )<sup>202</sup> is likely the cause of the diminished performance relative to **33-Dy** ( $n = 2.31$ ).<sup>201</sup> The role of spin-spin coupling between the 4f and 5d electron in **34-Tb** precludes definitive conclusions about these molecules.<sup>202,207</sup>

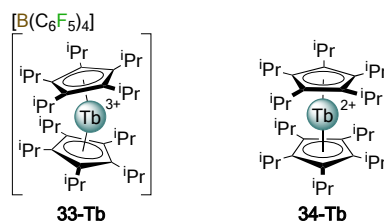


**Figure 11.** a)  $[\text{Tb}^{3+}(\text{Cp}^{\text{iPr}5})_2][\text{B}(\text{C}_6\text{F}_5)_4]$  (**33-Tb**); b)  $[\text{Tb}^{2+}(\text{Cp}^{\text{iPr}5})_2]$  (**34-Tb**).  $\text{Cp}^{\text{iPr}5} = \{\text{C}_5\text{iPr}_5\}$ .

A study of the magnetostructural relationship in a series of  $[\text{Dy}(\text{Cp}^{\text{iPr}4\text{R}})_2]^+$  cations ( $\text{Cp}^{\text{iPr}4\text{R}} = \{\text{C}_5\text{iPr}_4\text{R}\}$ ;  $\text{R} = \text{H}$ , **35-Dy**;  $\text{Me}$ , **36-Dy**;  $\text{Et}$ , **37-Dy**;  $\text{iPr}$ , **33-Dy**, Figure 12) by Long and Harvey has demonstrated the importance of replacing ring C–H groups with alkylated substituents,<sup>196</sup> as well as the fine interplay between ligand steric bulk and magnetic properties in these metallocenium cations.<sup>201,202</sup> All four homoleptic  $[\text{Dy}(\text{Cp}^{\text{iPr}4\text{R}})_2]^+$  complexes were synthesized analogously to **33-Dy** (where  $\text{R} = \text{iPr}$ ).<sup>201</sup> As previously described, increasing the *axiality* ( $\text{Cp}\cdots\text{Dy}\cdots\text{Cp}$  angle), and the *strength* ( $\text{Cp}^{\text{R}}_{\text{centroid}}/\text{C}\cdots\text{Dy}$  distances) of the ligand field will lead to purer  $m_{\text{J}}$  states with larger separations. The result of these synergic effects is that  $U_{\text{eff}}$  is ordered from  $\text{R} = \text{H}$  (**35-Dy**, 1,285  $\text{cm}^{-1}$ ),  $\text{iPr}$  (**33-Dy**, 1,334  $\text{cm}^{-1}$ ),  $\text{Et}$  (**37-Dy**, 1,380  $\text{cm}^{-1}$ ),  $\text{Me}$  (**36-Dy**, 1,468  $\text{cm}^{-1}$ ). Indeed the complex with the highest  $U_{\text{eff}}$  (**36-Dy**) has the second smallest  $\text{Cp}^{\text{R}}\cdots\text{Dy}\cdots\text{Cp}^{\text{R}}$  angle ( $156.6(3)^{\circ}$  for **36-Dy** vs  $147.2(8)^{\circ}$  for **35-Dy**;  $161.1(2)^{\circ}$  for **37-Dy**;  $162.1(7)^{\circ}$  for **33-Dy**) but also the second shortest average  $\text{Cp}^{\text{R}}\cdots\text{Dy}$  distances. All four complexes showed low Raman exponents (range 2.00 to 3.02) typical of  $\text{Ln}^{3+}$  metallocenium cations.<sup>196-202</sup> The  $T_{\text{H}}$  values (**35-Dy**, 32 K; **33-Dy**, 66 K; **37-Dy**, 66 K; **36-Dy**, 72 K) are exceptional, with three of these examples outperforming **32-Dy**.<sup>196,198</sup> It is clear that the  $T_{\text{H}}$  values and  $U_{\text{eff}}$  correlate very well for three of these complexes; though **35-Dy**, where  $\text{R} = \text{H}$ , has a distinctly low  $T_{\text{H}}$  (32 K) compared to the  $U_{\text{eff}}$ . Complex **35-Dy** has a significantly larger zero-field step in the hysteresis trace than the others in this series, which is not removed fully by diamagnetic dilution; thus, it is likely that hyperfine coupling, ligand vibrational modes, or increased transverse anisotropy leading to QTM are more important than stray dipolar fields for this complex.

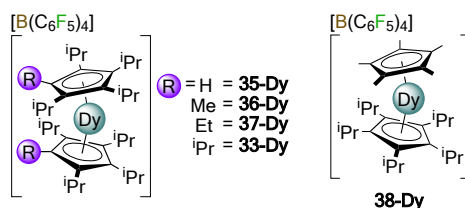


**Figure 12.** a) Schematic of the  $[\text{Dy}(\text{Cp}^{\text{iPr}4\text{R}})_2][\text{B}(\text{C}_6\text{F}_5)_4]$  ( $\text{Cp}^{\text{iPr}4\text{R}} = \{\text{C}_5\text{iPr}_4\text{R}\}$ ;  $\text{R} = \text{H}$ , **35-Dy**;  $\text{R} = \text{Me}$ , **36-Dy**;  $\text{R} = \text{Et}$ , **37-Dy**;  $\text{R} = \text{iPr}$ , **33-Dy**) series; b)  $[\text{Dy}(\text{Cp}^{\text{iPr}5})(\text{Cp}^*)][\text{B}(\text{C}_6\text{F}_5)_4]$  (**38-Dy**).

With the significance of the  $[\text{Dy}(\text{Cp}^{\text{R}})_2]^+$  framework established, refinements to the motif could be made to through judicious choice of the  $\text{Cp}^{\text{R}}$  ligands. By combining two different  $\text{Cp}^{\text{R}}$  ligands, Tong, Mansikkamäki, and Layfield synthesized  $[\text{Dy}(\text{Cp}^{\text{iPr5}})(\text{Cp}^*)][\text{B}(\text{C}_6\text{F}_5)_4]$  (**38-Dy**, Figure 12), which met all three requirements: 1) fully substituted  $\text{Cp}^{\text{R}}$  ligands remove the low energy C–H modes present in **32-Dy**; 2) the large steric profile of a  $\{\text{Cp}^{\text{iPr5}}\}$  ligand ensures there are no equatorial interactions; 3) the  $\{\text{Cp}^*\}$  ligand is significantly smaller than the  $\{\text{Cp}^{\text{iPr4R}}\}$  ligands used in **33-Dy** to **37-Dy**, which reduces inter-ligand repulsion allowing closer approach to the metal.<sup>208</sup> The  $\text{Cp}^{\text{R}}\cdots\text{Dy}\cdots\text{Cp}^{\text{R}}$  angle of **38-Dy** ( $162.51(1)^\circ$ ) is larger than all other isolated  $[\text{Dy}(\text{Cp}^{\text{R}})_2]^+$  cations (**32-Dy** to **37-Dy**; range:  $147.2(8)^\circ$  to  $162.1(7)^\circ$ ), while the  $\text{Cp}^{\text{R}}_{\text{centroid}}\cdots\text{Dy}$  distances ( $2.296(1)$  Å and  $2.284(1)$  Å) are the shortest observed. AC and DC magnetization measurements of relaxation times gave  $U_{\text{eff}} = 1,541$   $\text{cm}^{-1}$ ,  $n = 3.0$  and  $T_{\text{B2}} = 65$  K ( $T_{\text{irrev}} = 78$  K) for **38-Dy**, and hysteresis measurements show  $T_{\text{H}} = 80$  K,<sup>208</sup> which is above the boiling point of liquid nitrogen. Impressively, even at 77 K the lifetime is approximately 50 seconds. *Ab initio* calculations of the electronic structure showed the first six KDs well-described as  $m_{\text{J}} = \pm 15/2, \pm 13/2, \pm 11/2, \pm 9/2, \pm 7/2, \pm 5/2$ . The 5<sup>th</sup> and 6<sup>th</sup> KDs ( $m_{\text{J}} = \pm 7/2, \pm 5/2$ ) have non-negligible transverse components (though  $< 5\%$ ) and are thus likely responsible for relaxation in the high-temperature regime, indeed the  $U_{\text{eff}}$ , and the energy of the 5<sup>th</sup> KD ( $m_{\text{J}} = 7/2, 2,188$  K) are in modest agreement. Interestingly, while **32-Dy** relaxes *via* the 5<sup>th</sup> excited KD, **38-Dy** appears to only reach the 4<sup>th</sup> KD, though the significantly larger separation between the KDs results in a larger  $U_{\text{eff}}$  overall. Table 3 summarizes some properties of the  $[\text{Dy}(\text{Cp}^{\text{R}})_2]^+$  complexes discussed here. This hints at many subtle effects that interrelate, and further examples of the  $[\text{Dy}(\text{Cp}^{\text{R}})_2]^+$  family need to be exhaustively studied theoretically and experimentally.<sup>113,186</sup>

**Table 3.** Structural and magnetic parameters for six reported  $[\text{Dy}(\text{Cp}^{\text{R}})_2]^+$  cations.

	$T_{\text{H}} / \text{K}$	$U_{\text{eff}} / \text{cm}^{-1}$	$T_{\text{B2}} / \text{K}$	$\text{Cp}_{\text{cent}}\cdots\text{Dy}\cdots\text{Cp}_{\text{cent}} / ^\circ$ †	$\text{Dy}\cdots\text{C}_{\text{pcent}} / \text{Å}$ ‡
<b>38-Dy</b>	80	1,541	67	162.50(12)	2.284(4) / 2.296(3) <sup>§</sup>
<b>36-Dy</b>	72	1,468	64	156.6(3)	2.298(5)
<b>37-Dy</b>	66	1,380	57	161.1(2)	2.302(6)
<b>33-Dy</b>	66	1,334	59	162.1(7)	2.340(7)
<b>32-Dy</b>	60	1,223	56	152.56(7)	2.316(3)
<b>35-Dy</b> †	32	1,285	18	147.2(8)	2.29(1)

† Averages have been used across disordered parts. ‡ The average of the highest-occupancy part has been used. § The value of each ring has been given as the complex is heteroleptic.

### Conclusions and outlook

It has taken substantial synthetic advances to realize molecules that are remotely close to what theoreticians have envisaged in the field of Ln SMM chemistry.<sup>180,196,198,201,202</sup> The themes of symmetry and fine control of coordination chemistry are present throughout the field, though attention should be brought to a cautionary note. Complexes that feature perfect  $D_{5h}$  or  $D_{5d}$  symmetry are a physical impossibility in a real crystalline compound as five-fold symmetry is not possible in a *periodic solid*, and any complex with five non-identical equatorial donors cannot be described as having genuine five-fold symmetry. Therefore, QTM is not suppressed by

symmetry in such complexes, and over-stating point group symmetry can lead to misconceptions. Improvements in performance (such as improved coercivity or  $T_H$ ) could otherwise be rationalised through reduced mixing of states or by modification of the ligand vibrational modes and their influence within the Raman regime. It seems useful to target point groups that are achievable which also lead to cancellation of crystal field terms such as  $D_{4d}$  and  $D_{6d}$ .<sup>17</sup>

Given that a series of structurally similar  $[\text{Dy}(\text{Cp}^R)_2]^+$  cations have now been reported which represent a pinnacle in not just  $U_{\text{eff}}$ , but in crucial metrics that would define information storage (such as  $T_{B2}$ ), it is useful to try and see if there are magnetostructural trends. Table 3 shows that for most of these complexes,  $U_{\text{eff}}$  is closely correlated with  $T_H$  and  $T_{B2}$ , thus it seems likely there is an intrinsic link between structure and performance in this class of complex though clearly further studies are necessary to tease out any predictive models.<sup>100,186,201</sup>

More high-temperature SMMs are required to further our understanding, and several classes of molecules show excellent potential here. The tunability of carbocyclic systems in both charge and steric profile, will likely continue to afford innovative new molecular designs. For example, the cyclobutadiene dianion  $\{\text{C}_4(\text{R})_4\}^{2-}$  is an attractive target due to the high charge density which should produce strong crystal fields. It has proven problematic to install on lanthanides, leading to ligand non-innocence when homoleptic complexes have been targeted,<sup>209,210</sup> though heteroleptic molecules such as **39** (Figure 13) could prove useful. Other exciting avenues include exchanging C-atoms within the ring in order to drastically change the vibrational modes available in hetero-metalloeniums,<sup>211</sup> or in heteroleptic sandwich complexes.<sup>212</sup> While complexes that feature a  $\text{Cp}^R$  ligand bridging two Ln ions through all five C-atoms have been reported, for example a Gd– $\text{Cp}^*$ –Sm linkage in  $[\text{Gd}\{\text{OSi}(\text{O}^i\text{Bu})_3\}_3(\mu:\eta^5:\eta^5\text{-Cp}^*)\text{Sm}\{\text{OSi}(\text{O}^i\text{Bu})_3\}_3\text{Sm}]$  (**40**),<sup>213</sup> no study yet appears to have measured Ln···Ln superexchange coupling through  $\text{Cp}^R$  rings; however, a study on the  $\{\text{C}_7\text{H}_7\}^{3-}$  trianion showed related systems can have significant coupling.<sup>214</sup> The use of multiply-charged carbocycles such as  $\{\text{C}_4\text{R}_4\}^{2-}$ ,  $\{\text{C}_6\text{R}_6\}^{2-}$ ,  $\{\text{C}_7\text{R}_7\}^{3-}$  (R = alkyl, aryl, silyl, H, etc)<sup>215</sup> could afford highly-axial complexes where a closed-shell anionic bridging ligand is on-axis (**41**, Figure 13) and thus produce large  $U_{\text{eff}}$  values in coupled systems. Another attractive approach is to continue the development of radically-coupled systems. To date, the majority of such Ln-radical systems have used the  $\{\text{BPh}_4\}^-$  salts of  $\{\text{Ln}(\text{Cp}^R)_2\}^+$  precursors,<sup>156-158</sup> or were accessed by reduction of **20-Ln** complexes.<sup>152-154</sup> There is a problem with this as a near-ideal ligand field exists in the  $\{\text{Ln}(\text{Cp}^R)_2\}^+$  precursor and the radical bridge is orthogonal to the anisotropy axis for the  $m_J = \pm 15/2$  ground state in  $\text{Dy}^{3+}$  and is thus a detriment. The design of radically-bridged complexes where the bridge is on-axis, (or on the equator as necessary) as in **42** (Figure 13), could yield complexes where QTM is suppressed and also with  $U_{\text{eff}}$  sufficiently large enough to afford higher  $T_H/T_{B2}$  values. Such advances have previously been alluded to in Dy···Dy exchange systems which have anisotropy axis coincident with the Dy···Dy vector which leads to rare ferromagnetic direct exchange and suppression of QTM.<sup>148-151</sup>

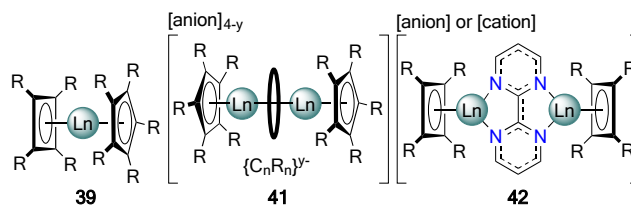


**Figure 13.** Proposed schematic complexes **39,41,42**, designed to maximize both  $U_{\text{eff}}$  and/or exchange interactions. R = alkyl, aryl, silyl, H, etc. and y is the charge on a bridging carbocyclic ring, e.g. for  $\{\text{C}_5\text{R}_5\}^{1-}$  y is 1. The reader is directed to a review in reference 215 by Diaconescu that includes rare-earth carbocycles and their charge states.

To conclude, after more than 25 years of concerted collaborative effort between theoreticians and synthetic chemists, the challenge set forth in 1993 to store information at the molecular level is closer to realization than ever before. Not only can magnetization be retained above 4 K, it can be done for measurable periods even at the boiling point of liquid nitrogen. The path forward requires new synthetic strategies, and new models need be devised to explain the current gaps in our knowledge. If an SMM is to ever sit in a commercial magnetic storage device, we likely need lifetimes of years at acceptable temperatures (ideally above 300 K) and ways to address individual spins. These challenges will hopefully inspire groups of theoreticians, synthetic chemists, and physicists to continue the exploration of this fascinating class of molecule for years to come.

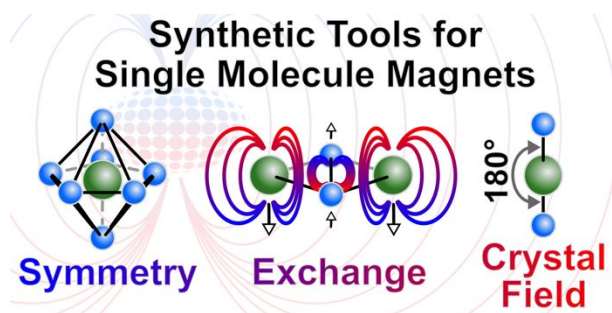
#### Conflicts of interest

There are no conflicts to declare.

#### Acknowledgements

The preparation of this manuscript was funded by the Laboratory Directed Research and Development program at Los Alamos National Laboratory through a J. Robert Oppenheimer Distinguished Postdoctoral Fellowship. I would like to thank Andrew J. Gaunt, David P. Mills, R. E. P. Winpenny, and Stephen T. Liddle for mentorship. I also thank Nicholas F. Chilton, Fabrizio Ortu, and Jon G. C. Kragoskow for proofreading. Finally, I thank H. Victoria Stafford for support and encouragement.

## Table of Contents



A synthetic chemists' guide to contemporary advances in the field of lanthanide single molecule magnetism.

## Photograph and Biography



Conrad Goodwin undertook both graduate and doctoral studies at the University of Manchester, completing a PhD in f-element silylamide chemistry with Dr David Mills in 2017. He then undertook a one-year EPSRC Doctoral Prize fellowship focussed on low-coordinate and low oxidation-state amido and organometallic lanthanide complexes as precursors to record-breaking single molecule magnets. In 2018 he subsequently moved to the United States to undertake a J. Robert Oppenheimer Distinguished Postdoctoral Fellowship at Los Alamos National Laboratory with Dr Andrew Gaunt. His research interests focus on the interrelation of oxidation state and covalency in transuranium elements, and on organometallic transuranium chemistry.

## References

---

1. C. J. Milios, *Single Molecule Magnets*, in *Reference Module in Chemistry, Molecular Sciences and Chemical Engineering*, Elsevier, 2019.
2. R. Sessoli, D. Gatteschi, A. Caneschi, M. A. Novak, *Nature*, 1993, **365**, 141–143.
3. T. Lis, *Acta Cryst.*, 1980, **B36**, 2042–2046.
4. J. Ferrando-Soria, J. Vallejo, M. Castellano, J. Martínez-Lillo, E. Pardo, J. Cano, I. Castro, F. Lloret, R. Ruiz-García, M. Julve, *Coord. Chem. Rev.*, 2017, **339**, 17–103.
5. E. Moreno-Pineda, C. Godfrin, F. Balestro, W. Wernsdorder, M. Ruben, *Chem. Soc. Rev.*, 2018, **47**, 501–513.
6. C. Godfrin, A. Ferhat, R. Ballou, S. Klyatskaya, M. Ruben, W. Wernsdorfer, F. Balestro, *Phys. Rev. Lett.*, 2017, **119**, 187702.
7. M. N. Leuenberger, D. Loss, *Nature*, 2001, **410**, 789–793.
8. D. Gatteschi, A. Cornia, M. Mannini, R. Sessoli, *Inorg. Chem.*, 2009, **48**, 3408–3419.
9. P. Zhang, L. Zhang, J. Tang, *Dalton Trans.*, 2015, **44**, 3923–3939.
10. Z. Zhu, M. Guo, Z.-L. Li, J. Tang, *Coord. Chem. Rev.*, 2019, **378**, 350–364.
11. P. Zhang, Y.-N. Guo, J. Tang, *Coord. Chem. Rev.*, 2013, **257**, 1728–1763.
12. J. Luzon, R. Sessoli, *Dalton Trans.*, 2012, **41**, 13556–13567.
13. O. Kahn, *Molecular Magnetism*, Wiley-Blackwell, New York, 1993.
14. D. Gatteschi, R. Sessoli, J. Villain, *Molecular Nanomagnets*, Oxford University Press, Oxford, 2006.
15. C. Bennelli, D. Gatteschi, *Introduction to Molecular Magnetism: From Transition Metals to Lanthanides*, Wiley-VCH Verlag GmbH & Co., Weinheim, 2015.
16. R. A. Layfield, M. Murugesu, *Lanthanides and Actinides in Molecular Magnetism*, Wiley-VCH Verlag GmbH & Co., Weinheim, 2015.
17. J.-L. Liu, Y.-C. Chen, M.-L. Tong, *Chem. Soc. Rev.*, 2018, **47**, 2431–2453.
18. M. Atanasov, D. Aravena, E. Sutura, E. Bill, D. Maganas, F. Neese, *Coord. Chem. Rev.*, 2015, **289-290**, 177–214.
19. A. F. Orchard, *Magnetochemistry*, Oxford University Press, Oxford, 2003.
20. L. Escalera-Moreno, J. J. Baldoví, A. Gaita-Ariño, E. Coronado, *Chem. Sci.*, 2018, **9**, 3265–3275.
21. J. Tang, P. Zhang, *Lanthanide Single Molecule Magnets*, Springer, 2015.
22. E. Coronado, *Nat. Rev. Mater.*, 2020, **5**, 87–104.
23. E. Coronado, P. Delhaès, D. Gatteschi, J. S. Miller, *Molecular Magnetism: From Molecular Assemblies to the Devices*, Springer, 1996.
24. M. Atzori, R. Sessoli, *J. Am. Chem. Soc.*, 2019, **141**, 11339–11351.
25. J. Lehmann, A. Gaita-Ariño, E. Coronado, D. Loss, *Nat. Nanotechnol.*, 2007, **2**, 312–317.
26. E. J. L. McInnes, R. E. P. Winpenny, in *Comprehensive Inorganic Chemistry II*, ed. J. Reedijk, K. Poeppelemeier, Elsevier, Amsterdam, 2013, 371–395.
27. R. Sessoli, A. K. Powell, *Coord. Chem. Rev.*, 2009, **253**, 2328–2341.
28. J. C. Goodwin, R. Sessoli, D. Gatteschi, W. Wernsdorfer, A. K. Powell, S. L. Heath, *J. Chem. Soc., Dalton Trans.*, 2000, 1835–1840.

- 
29. M. Murugesu, M. Habrych, W. Wernsdorfer, K. A. Abboud, G. Christou, *J. Am. Chem. Soc.*, 2004, **126**, 4766–4767.
30. A. M. Ako, I. J. Hewitt, V. Mereacre, R. Clérac, W. Wernsdorfer, C. E. Anson, A. K. Powell, *Angew. Chem., Int. Ed.*, 2006, **45**, 4926–4929.
31. S. Kang, H. Zheng, T. Liu, K. Hamachi, S. Kanegawa, K. Sugimoto, Y. Shiota, S. Hayami, M. Mito, T. Nakamura, M. Nakano, M. L. Baker, H. Nojiri, K. Yoshizawa, C. Duan, O. Sato, *Nat. Commun.*, 2015, **6**, 5955.
32. I. Aupiais, M. Mochizuki, H. Sakata, R. Grasset, Y. Gallais, A. Sacuto, M. Cazayous, *npj Quant. Mater.*, 2018, **3**, 60.
33. C. J. Milios, R. E. P. Winpenny, in *Molecular Nanomagnets and Related Phenomena. Structure and Bonding*, ed. S. Gao, Springer, Berlin, vol 164, 2014, 1–109.
34. W.-P. Chen, J. Singleton, L. Qin, A. Camón, L. Engelhardt, F. Luis, R. E. P. Winpenny, Y.-Z. Zheng, *Nat. Commun.*, 2018, **9**, 2107.
35. F. Neese, D. A. Pantazis, *Faraday Discuss.*, 2011, **148**, 229–238.
36. N. Ishikawa, M. Sugita, T. Ishikawa, S. Koshihara, Y. Kaizu, *J. Am. Chem. Soc.*, 2003, **125**, 8694–8695.
37. C. Loosli, S.-X. Liu, A. Neels, G. Labat, S. Decurtins, *Z. Kristallogr.*, 2006, **221**, 135–141.
38. D. N. Woodruff, R. E. P. Winpenny, R. A. Layfield, *Chem. Rev.*, 2013, **113**, 5110–5148.
39. J. Lu, M. Guo, J. Tang, *Chem. Asian J.*, 2017, **12**, 2772–2779.
40. J. M. Zadrozny, D. J. Xiao, M. Atanasov, G. J. Long, F. Grandjean, F. Neese, J. R. Long, *Nat. Chem.*, 2013, **5**, 577–581.
41. J. M. Zadrozny, M. Atanasov, A. M. Bryan, C.-Y. Lin, B. D. Reken, P. P. Power, F. Neese, J. R. Long, *Chem. Sci.*, 2013, **4**, 125–138 and references therein.
42. P. C. Bunting, M. Atanasov, E. Damgaard-Møller, M. Perfetti, I. Crassee, M. Orlita, J. Overgaard, J. van Slageren, F. Neese, J. R. Long, *Science*, 2018, **362**, eaat7319.
43. M. Feng, M.-L. Tong, *Chem. Eur. J.* 2018, **24**, 7574–7594.
44. H. Zhang, R. Nakanishi, K. Katoh, B. K. Breedlove, Y. Kitagawa, M. Yamashita, *Dalton Trans.*, 2018, **47**, 302–305.
45. A. J. Brown, D. Pinkowicz, M. R. Saber, K. R. Dunbar, *Angew. Chem., Int. Ed.*, 2015, **54**, 5864–5868.
46. S. T. Liddle, J. van Slageren, *Chem. Soc. Rev.*, 2015, **44**, 6655–6669.
47. R. A. Layfield, *Organometallics*, 2014, **33**, 1084–1099.
48. F.-S. Guo, A. K. Bar, R. A. Layfield, *Chem. Rev.*, 2019, **119**, 8479–8505 and references therein.
49. K. L. M. Harriman, D. Errulat, M. Murugesu, *Trends Chem.*, 2019, **1**, 425–439.
50. J. M. Frost, L. M. Harriman, M. Murugesu, *Chem. Sci.*, 2016, **7**, 2470–2491.
51. A. K. Bar, P. Kalita, M. K. Singh, G. Rajaraman, V. Chandrasekhar, *Coord. Chem. Rev.*, 2018, **367**, 163–216.
52. J. Wang, M. Feng, M. N. Akhtar, M.-L. Tong, *Coord. Chem. Rev.*, 2019, **387**, 129–153.
53. F. Pointillart, O. Cador, B. Le Guennic, L. Ouahab, *Coord. Chem. Rev.*, 2017, **346**, 150–175.
54. D. Shao, X.-Y. Wang, *Chin. J. Chem.*, 2020, **38**, 1005–1018.
55. A. K. Bar, C. Pichon, J.-P. Sutter, *Coord. Chem. Rev.* 2016, **308**, 346–380.
56. J. D. Rinehart, J. R. Long, *Chem. Sci.*, 2011, **2**, 2078–2085.
57. Sievers Plot: <https://kragoskow.com/sievers/>, (accessed May 2020).

- 
58. D. Aravena, E. Ruiz, *Dalton Trans.*, 2020, **49**, 9916–9928.
59. The same phenomena lead to decoherence in qubits, see: E. Garlatti, L. Tesi, A. Lunghi, M. Atzori, D. J. Voneshen, P. Santini, S. Sanvito, T. Guidi, R. Sessoli, S. Carretta, *Nat. Commun.*, 2020, **11**, 1751.
60. F. D. Natterer, K. Yang, W. Paul, P. Willke, T. Choi, T. Greber, A. J. Heinrich, C. P. Lutz, *Nature*, 2017, **543**, 226–228.
61. F. Donati, R. Rusponi, S. Stepanow, C. Wäckerlin, A. Singha, L. Persichetti, R. Baltic, K. Diller, F. Patthey, E. Fernandes, J. Dreiser, Ž. Šljivančanin, K. Kummer, C. Nistor, P. Gambardella, H. Brune, *Science*, 2016, **352**, 318–321.
62. J. Sievers, *Z. Phys. B: Condens. Matter Quanta*, 1982, **45**, 289–296.
63. L. Ungur, L. F. Chibotaru, *Phys. Chem. Chem. Phys.*, 2011, **13**, 20086–20090.
64. L. Ungur, L. F. Chibotaru, *Inorg. Chem.*, 2016, **55**, 10043–10056.
65. N. Ishikawa, M. Sugita, W. Wernsdorfer, *J. Am. Chem. Soc.*, 2005, **127**, 3650–3651.
66. Y.-C. Chen, J.-L. Liu, W. Wernsdorfer, D. Liu, L. F. Chibotaru, X.-M. Chen, M.-L. Tong, *Angew. Chem., Int. Ed.*, 2017, **56**, 4996–5000.
67. E. Moreno-Pineda, G. Taran, W. Wernsdorfer, M. Ruben, *Chem. Sci.*, 2019, **10**, 5138–5145.
68. W. J. Childs, *Phys. Rev. A*, 1970, **2**, 1692–1701.
69. F. Pointillart, K. Bernot, S. Golhen, B. Le Guennic, T. Guizouarn, L. Ouahab, O. Cador, *Angew. Chem., Int. Ed.*, 2015, **54**, 1504–1507.
70. Y. Kishi, F. Pointillart, B. Lefeuvre, F. Riobé, B. Le Guennic, S. Golhen, O. Cador, O. Maury, H. Fijuwara, L. Ouahab, *Chem. Commun.*, 2017, **53**, 3575–3578.
71. J. F. Gonzalez, F. Pointillart, O. Cador, *Inorg. Chem. Front.*, 2019, **6**, 1081–1086.
72. G. Huang, X. Yi, J. Jung, O. Guillou, O. Cador, F. Pointillart, B. Le Guennic, K. Bernot, *Eur. J. Inorg. Chem.*, 2018, 326–332.
73. F. Ortu, D. Reta, Y.-S. Ding, C. A. P. Goodwin, M. P. Gregson, E. J. L. McInnes, R. E. P. Winpenny, Y.-Z. Zheng, S. T. Liddle, D. P. Mills, N. F. Chilton, *Dalton Trans.*, 2019, **48**, 8541–8545.
74. Y. S. Ding, K.-X. Yu, D. Reta, F. Ortu, R. E. P. Winpenny, Y.-Z. Zheng, N. F. Chilton, *Nat. Commun.*, 2018, **9**, 3134.
75. K.-X. Yu, J. G. C. Kragsskow, Y.-S. Ding, Y.-Q. Zhai, D. Reta, N. F. Chilton, Y.-Z. Zheng, *Chem*, 2020, **6**, 1777–1793.
76. K. Irländer, J. Schnack, *Phys. Rev. B*, 2020, **102**, 054407. 1
77. N. Ishikawa, *Phthalocyanine-Based Magnets*, in *Functional Phthalocyanine Molecular Materials. Structure and Bonding*, ed. J. Jiang, Springer, Berlin, 2010, vol. 135.
78. Y. Chen, F. Ma, X. Chen, B. Dong, K. Wang, S. Jiang, C. Wang, X. Chen, D. Qi, H. Sun, B. Wang, S. Gao, J. Jiang, *Inorg. Chem. Front.*, 2017, **4**, 1465–1471.
79. C. Liu, M. Li, Y. Zhang, H. Tian, Y. Chen, H. Wang, J. Dou, J. Jiang, *Eur. J. Inorg. Chem.*, 2019, 2940–2946.
80. Y. Chen, F. Ma, X. Chen, Y. Zhang, H. Wang, K. Wang, D. Qi, H.-L. Sun, J. Jiang, *Inorg. Chem.*, 2019, **58**, 2422–2429.
81. M. A. Al Damen, J. M. Clemente-Juan, E. Coronado, C. Martí-Gastaldo, A. Gaita-Ariño, *J. Am. Chem. Soc.*, 2008, **130**, 8874–8875.

- 
82. M. A. Al Damen, S. Cardona-Serra, J. M. Clemente-Juan, E. Coronado, A. Gaita-Ariño, C. Martí-Gastaldo, F. Luis, O. Montero, *Inorg. Chem.*, 2009, **48**, 3467–3479.
83. K. Liu, X. Zhang, X. Meng, W. Shi, P. Cheng, A. K. Powell, *Chem. Soc. Rev.*, 2016, **45**, 2423–2439 and references therein.
84. D. I. Alexandropoulos, T. N. Nguyen, L. Cunha-Silva, T. F. Zafiroopoulos, A. Escuer, G. Christou, T. C. Stamatatos, *Inorg. Chem.*, 2013, **52**, 1179–1181.
85. A. Saha, M. Thompson, K. A. Abboud, W. Wernsdorfer, G. Christou, *Inorg. Chem.*, 2011, **50**, 10476–10485.
86. C. Papatrifiantafyllopoulou, W. Wernsdorfer, K. A. Abboud, G. Christou, *Inorg. Chem.*, 2011, **50**, 421–423.
87. T. C. Stamatatos, S. J. Teat, W. Wernsdorfer, G. Christou, *Angew. Chem., Int. Ed.*, 2009, **48**, 521–524.
88. W. Huang, J. J. Le Roy, S. I. Khan, L. Ungur, M. Murugesu, P. L. Diaconescu, *Inorg. Chem.*, 2015, **54**, 2374–2382.
89. R. J. Blagg, L. Ungur, F. Tuna, J. Speak, P. Comar, D. Collison, W. Wernsdorfer, E. J. L. McInnes, L. F. Chibotaru, R. E. P. Winpenny, *Nat. Chem.*, 2013, **5**, 673–678.
90. M. T. Gamer, Y. Lan, P. W. Roesky, A. K. Powell, R. Clérac, *Inorg. Chem.*, 2008, **47**, 6581–6583.
91. Y.-Z. Zheng, Y. Lan, C. E. Anson, A. K. Powell, *Inorg. Chem.*, 2008, **47**, 10813–10815.
92. J. Tang, I. Hewitt, N. T. Madhu, G. Chastanet, W. Wernsdorfer, C. E. Anson, C. Benelli, R. Sessoli, A. K. Powell, *Angew. Chem., Int. Ed.*, 2006, **45**, 1729–1733.
93. P.-H. Lin, T. J. Burchell, L. Ungur, L. F. Chibotaru, W. Wernsdorfer, M. Murugesu, *Angew. Chem., Int. Ed.*, 2009, **48**, 9489–9492.
94. [Tb(Pc)<sub>2</sub>] and derivatives are useful for spintronics research, see: K. Katoh, H. Isshiki, T. Komeda, M. Yamashita, *Chem. Asian J.*, 2012, **7**, 1154–1169 for a review.
95. C. Liu, M. Li, Y. Zhang, H. Tian, Y. Chen, H. Wang, J. Dou, J. Jiang, *Eur. J. Inorg. Chem.*, 2019, 2940–2946.
96. Y. S. Meng, S. D. Jiang, B.-W. Wang, S. Gao, *Acc. Chem. Res.*, 2016, **49**, 2381–2389.
97. N. F. Chilton, D. Collison, E. J. L. McInnes, R. E. P. Winpenny, A. Soncini, *Nat. Commun.*, 2013, **4**, 2551.
98. L. Escalera-Moreno, J. J. Baldovi, A. Gaita-Ariño, E. Coronado, *Inorg. Chem.*, 2019, **58**, 11883–11892.
99. Y.-N. Guo, G.-F. Xu, Y. Guo, J. Tang, *Dalton Trans.*, 2011, **40**, 9953–9963.
100. N. F. Chilton, *Inorg. Chem.*, 2015, **54**, 2097–2099.
101. See R. Marin, G. Brunet, M. Murugesu, *Angew. Chem., Int. Ed.*, 2019, DOI: 10.1002/anie.201910299 and references therein.
102. M. Xémard, M. Cordier, F. Molton, C. Duboc, B. Le Guennic, O. Maury, O. Cador, G. Nocton, *Inorg. Chem.*, 2019, **58**, 2872–2880.
103. P.-E. Car, M. Perfetti, M. Mannini, A. Favre, A. Caneschi, R. Sessoli, *Chem. Commun.*, 2011, **47**, 3751–3753.
104. G. Cucinotta, M. Perfetti, J. Luzon, M. Etienne, P.-E. Car, A. Caneschi, G. Calvez, K. Bernot, R. Sessoli, *Angew. Chem., Int. Ed.*, 2012, **51**, 1606–1610.
105. D. Reta, N. F. Chilton, *Phys. Chem. Chem. Phys.*, 2019, **21**, 23567–23575.

- 
106. J. D. Hilgar, A. K. Butts, J. D. Rinehart, *Phys. Chem. Chem. Phys.*, 2019, **21**, 22302–22307.
107. C. V. Topping and S. J. Blundell, *J. Phys.: Condens. Matter*, 2019, **31**, 013001.
108. M. J. Giansiracusa, A. K. Kostopoulos, D. Collison, R. E. P. Winpenny, N. F. Chilton, *Chem. Commun.*, 2019, **55**, 7025–7028.
109. P. L. Scott, C. D. Jeffries, *Phys. Rev.*, 1962, **127**, 32–51.
110. E. Lucaccini, L. Sorace, M. Perfetti, J.-P. Costes, R. Sessoli, *Chem. Commun.*, 2014, **50**, 1648–1651.
111. C. A. P. Goodwin, F. Ortu, D. Reta, *Int. J. Quantum Chem.*, 2020, **120**, e26248.
112. E. J. L. McInnes in *Single-Molecule Magnets and Related Phenomena*, ed. R. E. P. Winpenny, Springer-Verlag, Berlin, 2006.
113. A. Chiesa, F. Cugini, R. Hussain, E. Macaluso, G. Allodi, E. Garlatti, M. Giansiracusa, C. A. P. Goodwin, F. Ortu, D. Reta, J. M. Skelton, T. Guidi, P. Santini, M. Solzi, R. De Renzi, D. P. Mills, N. F. Chilton, and S. Carretta, *Phys. Rev. B*, 2020, **101**, 174402.
114. S.-D. Jiang, B.-W. Wang, G. Su, Z.-M. Wang, S. Gao, *Angew. Chem., Int. Ed.*, 2010, **49**, 7448–7451.
115. S.-D. Jiang, B.-W. Wang, H.-L. Sun, Z.-M. Wang, S. Gao, *J. Am. Chem. Soc.*, 2011, **133**, 4730–4733.
116. S.-D. Jiang, S.-S. Liu, L.-N. Zhou, B.-W. Wang, Z.-M. Wang, S. Gao, *Inorg. Chem.*, 2012, **51**, 3079–3087.
117. K. R. Meihaus, J. R. Long, *J. Am. Chem. Soc.*, 2013, **135**, 17952–17957.
118. L. Ungur, J. J. Le Roy, I. Korobkov, M. Murugesu, L. F. Chibotaru, *Angew. Chem., Int. Ed.*, 2014, **53**, 4413–4417.
119. P. G. Jones, C. G. Hrib, T. K. Panda, M. Tamm, *Acta Crystallogr.*, 2007, **E63**, m2059.
120. J. Xia, Z. Jin, W. Chen, *J. Chem. Soc., Chem. Commun.*, 1991, 1214–1215.
121. P. Poremba, F. T. Edelmann, *J. Organomet. Chem.*, 1998, **553**, 393–395.
122. J. J. Le Roy, I. Korobkov, M. Murugesu, *Chem. Commun.*, 2014, **50**, 1602–1604.
123. J. J. Le Roy, L. Ungur, I. Korobkov, L. F. Chibotaru, M. Murugesu, *J. Am. Chem. Soc.*, 2014, **136**, 8003–8010.
124. J. J. Le Roy, M. Jeletic, S. I. Gorelsky, L. Korobkov, L. Ungur, L. F. Chibotaru, M. Murugesu, *J. Am. Chem. Soc.*, 2013, **135**, 3502–3510.
125. L. Münzfeld, C. Schoo, S. Bestgen, E. Moreno-Pineda, R. Köppe, M. Ruben, P. W. Roesky, *Nat. Commun.*, 2019, **10**, 3135.
126. M. Xémar, S. Zimmer, M. Cordier, V. Goudy, L. Ricard, C. Clavaguéra, G. Nocton, *J. Am. Chem. Soc.*, 2018, **140**, 14433–14439.
127. J. J. Baldoví, S. Cardona-Serra, J. M. Clemente-Juan, E. Coronado, A. Gaita-Ariño, A. Palií, *Inorg. Chem.*, 2012, **51**, 12565–12574.
128. J. J. Baldoví, J. J. Borrás-Almenar, J. M. Clemente-Juan, E. Coronado, A. Gaita-Ariño, *Dalton Trans.*, 2012, **41**, 13705–13710.
129. N. F. Chilton, S. K. Langlely, B. Moubaraki, A. Soncini, S. R. Batten, K. S. Murray, *Chem. Sci.*, 2013, **4**, 1719–1730.
130. W. Wernsdorfer, N. Aliaga-Alcalde, D. N. Hendrickson, G. Christou, *Nature*, 2002, **416**, 406–409.
131. T. P. Latendresse, N. S. Bhuvanesh, M. Nippe, *J. Am. Chem. Soc.*, 2017, **139**, 8058–8061.

- 
132. T. P. Latendresse, V. Vieru, B. O. Wilkins, N. S. Bhuvanesh, L. F. Chibotaru, M. Nippe, *Angew. Chem., Int. Ed.*, 2018, **57**, 8164–8169.
133. T. P. Latendresse, V. Vieru, A. Upadhyay, N. S. Bhuvanesh, L. Chibotaru, M. Nippe, *Chem. Sci.*, 2020, **11**, 3936–3951.
134. T. P. Latendresse, N. S. Bhuvanesh, M. Nippe, *J. Am. Chem. Soc.*, 2017, **139**, 14877–14880.
135. J. B. Goodenough, *J. Phys. Chem. Solids*, 1958, **6**, 287–297.
136. J. Kanamori, *J. Phys. Chem. Solids*, 1959, **10**, 87–98.
137. W. Geertsma, D. Khomskii, *Phys. Rev. B*, 1996, **54**, 3011–3014.
138. J. Long, F. Habib, P.-H. Lin, I. Korobkov, G. Enright, L. Ungur, W. Wernsdorfer, L. F. Chibotaru, M. Murugesu, *J. Am. Chem. Soc.*, 2011, **133**, 5319–5328.
139. P.-H. Lin, I. Korobkov, W. Wernsdorfer, L. Ungur, L. F. Chibotaru, M. Murugesu, *Eur. J. Inorg. Chem.*, 2011, 1535–1539.
140. G.-F. Xu, Q.-L. Wang, P. Gamez, Y. Ma, R. Clérac, J. Tang, S.-P. Yan, P. Cheng, D.-Z. Liao, *Chem. Commun.*, 2010, **46**, 1506–1508.
141. R. Grindell, B. M. Day, F.-S. Guo, T. Pugh, R. A. Layfield, *Chem. Commun.*, 2017, **53**, 9990–9993.
142. T. Pugh, N. F. Chilton, R. A. Layfield, *Angew. Chem., Int. Ed.*, 2016, **55**, 11082–11085.
143. R. Collins, M. J. Heras Ojea, A. Mansikkamäki, J. Tang, R. A. Layfield, *Inorg. Chem.*, 2020, **59**, 642–647.
144. T. Pugh, F. Tuna, L. Ungur, D. Collison, E. J. L. McInnes, L. F. Chibotaru, R. A. Layfield, *Nat. Commun.*, 2015, **6**, 7492.
145. T. Pugh, V. Vieru, L. F. Chibotaru, R. A. Layfield, *Chem. Sci.*, 2016, **7**, 2128–2137.
146. T. Pugh, N. F. Chilton, R. A. Layfield, *Chem. Sci.*, 2017, **8**, 2073–2080.
147. M. He, F.-S. Guo, J. Tang, A. Mansikkamäki, R. A. Layfield, *Chem. Sci.*, 2020, **11**, 5745–5752.
148. J. Lu, Y.-Q. Zhang, X.-L. Li, M. Guo, J. Wu, L. Zhao, J. Tang, *Inorg. Chem.*, 2019, **58**, 5715–5724.
149. Y.-N. Guo, G.-F. Xu, W. Wernsdorfer, L. Ungur, Y. Guo, J. Tang, H.-J. Zhang, L. F. Chibotaru, A. K. Powell, *J. Am. Chem. Soc.*, 2011, **133**, 11948–11951.
150. Y. Peng, V. Mereacre, A. Baniodeh, Y. Lan, M. Schlageter, G. E. Kostakis, A. K. Powell, *Inorg. Chem.*, 2016, **55**, 68–74.
151. Y. Horii, K. Katoh, K. Sugimoto, R. Nakanishi, B. K. Breedlove, M. Yamashita, *Chem. Eur. J.*, 2019, **25**, 3098–3104.
152. J. D. Rinehart, M. Fang, W. J. Evans, J. R. Long, *J. Am. Chem. Soc.*, 2011, **133**, 14236–14239.
153. J. D. Rinehart, M. Fang, W. J. Evans, J. R. Long, *Nat. Chem.*, 2011, **3**, 538–542.
154. S. Demir, M. I. Gonzalez, L. E. Darago, W. J. Evans, J. R. Long, *Nat. Commun.*, 2017, **8**, 2144.
155. W. J. Evans, M. Fang, G. Zucchi, F. Furche, J. W. Ziller, R. M. Hoekstra, J. I. Zink, *J. Am. Chem. Soc.*, 2009, **131**, 11195–11202.
156. S. Demir, J. M. Zadrozny, M. Nippe, J. R. Long, *J. Am. Chem. Soc.*, 2012, **134**, 18546–18549.
157. S. Demir, M. Nippe, M. I. Gonzalez, J. R. Long, *Chem. Sci.*, 2014, **5**, 4701–4711.
158. C. A. Gould, L. E. Darago, M. I. Gonzalez, S. Demir, J. R. Long, *Angew. Chem., Int. Ed.*, 2017, **56**, 10103–10107.

159. C. Chen, Z. Hu, J. Li, H. Ruan, Y. Zhao, G. Tan, Y. Song, X. Wang, *Inorg. Chem.*, 2020, **59**, 2111–2115.
160. W. W. Lukens, N. Magnani, C. W. Booth, *Inorg. Chem.*, 2012, **51**, 10105–10110.
161. W. J. Evans, C. A. Seibel, J. W. Ziller, *J. Am. Chem. Soc.*, 1998, **120**, 6745–6752.
162. S. Demir, J. M. Zadrozny, J. R. Long, *Chem. Eur. J.*, 2014, **20**, 9524–9529.
163. B. M. Day, F.-S. Guo, R. A. Layfield, *Acc. Chem. Res.*, 2018, **51**, 1880–1889.
164. Y.-S. Meng, Y.-Q. Zhang, Z.-M. Wang, B.-W. Wang, S. Gao, *Chem. Eur. J.*, 2016, **22**, 12724–12731.
165. S. Demir, M. D. Boshart, J. F. Corbey, D. H. Woen, M. I. Gonzalez, J. W. Ziller, K. R. Meihaus, J. R. Long, W. J. Evans, *Inorg. Chem.*, 2017, **56**, 15049–15056.
166. R. Collins J. P. Durrant, M. He, R. A. Layfield, *Electronic structure and magnetic properties of rare-earth organometallic sandwich compounds*, in *Handbook on the Physics and Chemistry of Rare Earths*, eds. J.-C. G. Bünzli, V. K. Pecharsky, Elsevier, vol. 55, 2019.
167. C. P. Burns, X. Yang, J. D. Wofford, N. S. Bhuvanesh, M. B. Hall, M. Nippe, *Angew. Chem., Int. Ed.*, 2018, **57**, 8144–8148.
168. S.-M. Chen, J. Xiong, Y.-Q. Zhang, F. Ma, H.-L. Sun, B.-W. Wang, S. Gao, *Chem. Commun.*, 2019, **55**, 8250–8253.
169. S. Demir, M. Nippe, M. I. Gonzalez, J. R. Long, *Chem. Sci.*, 2014, **5**, 4701–4711.
170. C. A. P. Goodwin, B. L. L. Réant, G. F. Vettese, J. G. C. Kragoskow, M. J. Giansiracusa, I. M. DiMucci, K. M. Lancaster, D. P. Mills, S. Sproules, *Inorg. Chem.*, 2020, **59**, 7571–7583.
171. C. R. Ganivet, B. Ballesteros, G. de la Torre, J. M. Clemente-Juan, E. Coronado, T. Torres, *Chem. Eur. J.*, 2013, **19**, 1457–1465.
172. H. L. C. Feltham, S. Brooker, *Coord. Chem. Rev.*, 2014, **276**, 1–33.
173. S. P. Willson, L. Andrews, *J. Phys. Chem. A*, 1999, **103**, 6972–6983.
174. P. Zhang, L. Zhang, C. Wang, S. Que, S.-Y. Lin, J. Tang, *J. Am. Chem. Soc.*, 2014, **136**, 4484–4487.
175. A. J. Brown, D. Pinkowicz, M. R. Saber, K. R. Dunbar, *Angew. Chem., Int. Ed.*, 2015, **54**, 5864–5868.
176. P. Zheng, J. Jung, L. Zhang, J. Tang, B. Le Guennic, *Inorg. Chem.*, 2016, **55**, 1905–1911.
177. N. F. Chilton, C. A. P. Goodwin, D. P. Mills, R. E. P. Winpenny, *Chem. Commun.*, 2015, **51**, 101–103.
178. C. A. P. Goodwin, N. F. Chilton, G. F. Vettese, E. Moreno Pineda, I. F. Crow, J. W. Ziller, R. E. P. Winpenny, W. J. Evans, D. P. Mills, *Inorg. Chem.*, 2016, **55**, 10057–10067.
179. C. A. P. Goodwin, B. L. L. Réant, J. G. C. Kragoskow, I. M. DiMucci, K. M. Lancaster, D. P. Mills, S. Sproules, *Dalton Trans.*, 2018, **47**, 10613–10625.
180. H. M. Nicholas, M. Vonci, C. A. P. Goodwin, S. W. Loo, S. R. Murphy, D. Cassim, R. E. P. Winpenny, E. J. L. McInnes, N. F. Chilton, D. P. Mills, *Chem. Sci.*, 2019, **10**, 10493–10502.
181. Y.-C. Chen, J.-L. Liu, L. Ungur, J. Liu, Q.-W. Li, L.-F. Wang, Z.-P. Ni, L. F. Chibotaru, X.-M. Chen, M.-L. Tong, *J. Am. Chem. Soc.*, 2016, **138**, 2829–2837.
182. S. K. Gupta, T. Rajeshkumar, G. Rajaraman, R. Murugavel, *Chem. Sci.*, 2016, **7**, 5181–5191.
183. M. Gregson, N. F. Chilton, A.-M. Ariciu, F. Tuna, I. F. Crowe, W. Lewis, A. J. Blake, D. Collison, E. J. L. McInnes, R. E. P. Winpenny, S. T. Liddle, *Chem. Sci.*, 2016, **7**, 155–165.
184. J. Liu, Y.-C. Chen, J.-L. Liu, V. Vieru, L. Ungur, J.-H. Jia, L. F. Chibotaru, Y. Lan, W. Wernsdorfer, S. Gao, X.-M. Chen, M.-L. Tong, *J. Am. Chem. Soc.*, 2016, **138**, 5441–5450.

- 
185. Y.-S. Ding, N. F. Chilton, R. E. P. Winpenny, Y.-Z. Zheng, *Angew. Chem., Int. Ed.*, 2016, **55**, 16071–16074.
186. Y.-S. Ding, T. Han, Y.-Q. Zhai, D. Reta, N. F. Chilton, R. E. P. Winpenny, Y.-Z. Zheng, *Chem. Eur. J.*, 2020, **26**, 5893–5902.
187. K. S. Pedersen, J. Dreiser, H. Weihe, R. Sibille, H. V. Johannesen, M. A. Sørensen, B. E. Nielsen, M. Sigrist, H. Mutka, S. Rols, J. Bendix, S. Piligkos, *Inorg. Chem.*, 2015, **54**, 7600–7606.
188. W. J. Evans, B. L. Davis, T. M. Champagne, J. W. Ziller, *Proc. Nat. Acad. Sci.*, 2006, **103**, 12678–12683.
189. A. Berkefeld, W. E. Piers, M. Parvez, L. Castro, L. Maron, O. Eisenstein, *J. Am. Chem. Soc.*, 2012, **134**, 10843–10851.
190. S. Kaita, Z. Hou, M. Nishiura, Y. Doi, J. Kurazumi, A. C. Horiuchi, Y. Wakatsuki, *Macromol. Rapid Commun.*, 2003, **24**, 179–184.
191. M. J. Heras Ojea, L. C. H. Maddock, R. A. Layfield, *Lanthanide Organometallics as Single-Molecule Magnets*, in *Organometallic Magnets*, ed. V. Chandrasekhar, F. Pointillart, Springer Nature, Switzerland, 2019.
192. C. P. Burns, B. O. Wilkins, C. M. Dickie, T. P. Latendresse, L. Vernier, K. R. Vignesh, N. S. Bhuvanesh, M. Nippe, *Chem. Commun.*, 2017, **53**, 8419–8422.
193. P. Evans, D. Reta, C. A. P. Goodwin, F. Ortu, N. F. Chilton, D. P. Mills, *Chem. Commun.*, 2020, **56**, 5677–5680.
194. D. Errulat, B. Gabidullin, A. Mansikkamäki, M. Murugesu, *Chem. Commun.*, 2020, **56**, 5937–5940.
195. F. Jaroschik, F. Nief, X.-F. Le Goff, L. Ricard, *Organometallics*, 2007, **26**, 1123–1125.
196. C. A. P. Goodwin, F. Ortu, D. Reta, N. F. Chilton, D. P. Mills, *Nature*, 2017, **548**, 439–442.
197. C. A. P. Goodwin, D. Reta, F. Ortu, N. F. Chilton, D. P. Mills, *J. Am. Chem. Soc.*, 2017, **139**, 18714–18724.
198. F.-S. Guo, B. M. Day, Y.-C. Chen, M.-L. Tong, A. Mansikkamäki, R. A. Layfield, *Angew. Chem., Int. Ed.*, 2017, **56**, 11445–11449.
199. C. A. P. Goodwin, D. Reta, F. Ortu, J. Liu, N. F. Chilton, D. P. Mills, *Chem. Commun.*, 2018, **54**, 9182–9185.
200. J. Liu, D. Reta, J. A. Cleghorn, Y. X. Yeoh, F. Ortu, C. A. P. Goodwin, N. F. Chilton, D. P. Mills, *Chem. Eur. J.*, 2019, **25**, 7749–7758.
201. K. R. McClain, C. A. Gould, K. Chakarawet, S. J. Teat, T. J. Groshens, J. R. Long, B. G. Harvey, *Chem. Sci.*, 2018, **9**, 8492–8503.
202. C. A. Gould, K. R. McClain, J. M. Yu, T. J. Groshens, F. Furche, B. G. Harvey, J. R. Long, *J. Am. Chem. Soc.*, 2019, **141**, 12967–12973.
203. C. Ruspic, J. R. Moss, M. Schürmann, S. Harder, *Angew. Chem., Int. Ed.*, 2008, **47**, 2121–2126.
204. S. Harder, D. Naglav, C. Ruspic, C. Wickleder, M. Adlung, W. Hermes, M. Eul, R. Pöttgen, D. B. Rego, F. Poineau, K. R. Czerwinski, R. H. Herber, I. Nowik, *Chem. Eur. J.*, 2013, **19**, 12272–12280.
205. R. P. Kelly, T. D. M. Bell, R. P. Cox, D. P. Daniels, G. B. Deacon, F. Jaroschik, P. C. Junk, X. F. Le Goff, G. Lemercier, A. Martinez, J. Wang, D. Werner, *Organometallics*, 2015, **34**, 5624–5636.
206. N. J. C. van Velzen, S. Harder, *Organometallics*, 2018, **37**, 2263–2271.
207. V. Dubrovin, A. A. Popov, S. Avdoshenko, *Chem. Commun.*, 2019, **55**, 13963–13966.

- 
208. F.-S. Guo, B. M. Day, Y.-C. Chen, M.-L. Tong, A. Mansikkamäki, R. A. Layfield, *Science*, 2018, **362**, 1400–1403.
209. N. Tsoureas, A. Mansikkamäki, R. A. Layfield, *Chem. Commun.*, 2020, **56**, 944–947.
210. A. Chakraborty, B. M. Day, J. P. Durrant, M. He, J. Tang, R. A. Layfield, *Organometallics*, 2020, **39**, 8–12.
211. P. Evans, D. Reta, G. F. S. Whitehead, N. F. Chilton, D. P. Mills, *J. Am. Chem. Soc.*, 2019, **141**, 19935–19940.
212. S.-M. Chen, J. Xiong, Y.-Q. Zhang, Q. Yuan, B.-W. Wang, S. Gao, *Chem. Sci.*, 2018, **9**, 7540–7545.
213. M. Nishiura, Z. Hou, Y. Wakatsuki, *Organometallics*, 2004, **23**, 1359–1368.
214. K. L. M. Harriman, J. J. Le Roy, L. Ungur, R. J. Holmberg, I. Korobkov, M. Murugesu, *Chem. Sci.*, 2017, **8**, 231–240.
215. W. Huang, P. L. Diaconescu, *Dalton Trans.*, 2015, **44**, 15360–15371.